Cell-cycle regulation of formin-mediated actin cable assembly

Yansong Miao[a], Catherine C. L. Wong[b,1], Vito Mennella[c,d], Alphée Michelot[a,2], David A. Agard[c,d], Liam J. Holt[a], John R. Yates III[b], and David G. Drubin[a,3]

[a]Department of Molecular and Cell Biology, University of California, Berkeley, CA 94720; [b]Department of Chemical Physiology, The Scripps Research Institute, La Jolla, CA 92037; and [c]Department of Biochemistry and Biophysics and [d]The Howard Hughes Medical Institute, University of California, San Francisco, CA 94158

Edited by Ronald D. Vale, University of California, San Francisco, CA, and approved September 18, 2013 (received for review July 25, 2013)

Assembly of appropriately oriented actin cables nucleated by formin proteins is necessary for many biological processes in diverse eukaryotes. However, compared with knowledge of how nucleation of dendritic actin filament arrays by the actin-related protein-2/3 complex is regulated, the in vivo regulatory mechanisms for actin cable formation are less clear. To gain insights into mechanisms for regulating actin cable assembly, we reconstituted the assembly process in vitro by introducing microspheres functionalized with the C terminus of the budding yeast formin Bni1 into extracts prepared from yeast cells at different cell-cycle stages. EM studies showed that unbranched actin filament bundles were reconstituted successfully in the yeast extracts. Only extracts enriched in the mitotic cyclin Clb2 were competent for actin cable assembly, and cyclin-dependent kinase 1 activity was indispensible. Cyclin-dependent kinase 1 activity also was found to regulate cable assembly in vivo. Here we present evidence that formin cell-cycle regulation is conserved in vertebrates. The use of the cable-reconstitution system to test roles for the key actin-binding proteins tropomyosin, capping protein, and cofilin provided important insights into assembly regulation. Furthermore, using mass spectrometry, we identified components of the actin cables formed in yeast extracts, providing the basis for comprehensive understanding of cable assembly and regulation.

Cdk1 | three-dimensional structured-illumination microscopy | actin nucleation

Eukaryotic cells contain populations of actin structures with distinct architectures and protein compositions, which mediate varied cellular processes (1). Understanding how F-actin polymerization is regulated in time and space is critical to understanding how actin structures provide mechanical forces for corresponding biological processes. Branched actin filament arrays, which concentrate at sites of clathrin-mediated endocytosis (2, 3) and at the leading edge of motile cells (4), are nucleated by the actin-related protein-2/3 (Arp2/3) complex. In contrast, bundles of unbranched actin filaments, which sometimes mediate vesicle trafficking or form myosin-containing contractile bundles, often are nucleated by formin proteins (5–14).

Much has been learned about how branched actin filaments are polymerized by the Arp2/3 complex and how these filaments function in processes such as endocytosis (2, 15). In contrast, relatively little is known about how actin cables are assembled under physiological conditions. In previous studies, branched actin filaments derived from the Arp2/3 complex have been reconstituted using purified proteins (16–19) or cellular extracts (20–25). When microbeads were coated with nucleation-promoting factors for the Arp2/3 complex and then were incubated in cell extracts, actin comet tails were formed by sequential actin nucleation, symmetry breaking, and tail elongation. Importantly, the motility behavior of F-actin assembled by the Arp2/3 complex using defined, purified proteins differs from that of F-actin assembled by the Arp2/3 complex in the full complexity of cytoplasmic extracts (19, 26–28).

Formin-based actin filament assembly using purified proteins also has been reported (29, 30). However, reconstitution of formin-derived actin cables under the more physiological conditions represented by cell extracts has not yet been reported.

The actin nucleation activity of formin proteins is regulated by an inhibitory interaction between the N- and C-terminal domains, which can be released when GTP-bound Rho protein binds to the formin N-terminal domain, allowing access of the C terminus (FH1-COOH) to actin filament barbed ends (31–40). In yeast, the formin Bni1 N terminus also has an inhibitory effect on actin nucleation through binding to the C terminus (41).

Interestingly, several recent reports provided evidence for cell-cycle regulation of F-actin dynamics in oocytes and early embryos (42–45). However, which specific types of actin structures are regulated by the cell cycle and what kind of nucleation factors and actin interacting-proteins are involved remain to be determined.

Here, we report a reconstitution of actin cables in yeast extracts from microbeads derivatized with Bni1 FH1-COOH, identifying the proteins involved, increasing the inventory of the proteins that regulate actin cable dynamics and establishing that the actin cable reconstitution in cytoplasmic extracts is cell-cycle regulated.

Results

Reconstitution of Bni1-Derived Actin Cable Assembly in Mitotic Yeast Extracts. To investigate the regulation and assembly of actin cables nucleated by formins, we took advantage of the yeast cytoplasmic

Significance

Actin filaments are protein polymers that facilitate multiple biological functions, including cell migration, vesicle trafficking, and polarity establishment in eukaryotic cells throughout the cell cycle. Mechanisms of spatial and temporal regulation of actin assembly in vivo are incompletely understood. Formin proteins nucleate cables, which are bundles of unbranched actin filaments. We developed a cell-extract system to reconstitute actin cable assembly nucleated by formins in a physiological context. Using this unique reconstitution system, we identified an actin cable parts list. We also discovered that actin cable assembly is regulated in a cell-cycle–dependent manner both in vivo and in vitro.

Author contributions: Y.M. and D.G.D. designed research; Y.M., C.C.L.W., and V.M. performed research; Y.M., A.M., D.A.A., L.J.H., J.R.Y., and D.G.D. analyzed data; and Y.M. and D.G.D. wrote the paper.

The authors declare no conflict of interest.

This article is a PNAS Direct Submission.

See Commentary on page 18744.

[1]Present address: National Center for Protein Science, Shanghai, Shanghai Institute of Biochemistry and Cell Biology, Chinese Academy of Sciences, Pudong, Shanghai 200031, People's Republic of China.

[2]Present address: Laboratoire de Physiologie Cellulaire et Végétale, Centre National de la Recherche Scientifique, Commissariat à l'Energie Atomique et aux Energies Alternatives, Université Grenoble Alpes, 38054 Grenoble, France.

[3]To whom correspondence should be addressed. E-mail: drubin@berkeley.edu.

This article contains supporting information online at www.pnas.org/lookup/suppl/doi:10.1073/pnas.1314000110/-/DCSupplemental.

extract system previously used to reconstitute Arp2/3-mediated actin filament assembly and introduced into these extracts polystyrene beads coated with the FH1-COOH (amino acids 1227–1954) domain of Bni1 (46). These beads were added to cytoplasmic extracts from yeast expressing Abp140 tagged with three molecules of GFP (Abp140-3×GFP) as an actin cable marker. Initially, we incubated the GST-Bni1 FH1-COOH–coated beads in extracts from unsynchronized log-phase yeast cells. Although Las17 (yeast WASP)-functionalized beads incubated in these extracts effectively formed actin comet tails (Fig. S1*A*) (24), no F-actin was detected in association with the GST-Bni1 FH1-COOH–coated beads (Fig. 1*A*).

Recently, F-actin assembly was found to be regulated by the cell cycle in vertebrates (43, 45). Actin bundles assembled in metaphase were thicker and/or more prevalent than those assembled in interphase (43). Cell-cycle regulation of actin assembly may be a conserved phenomenon because actin cables in fission yeast are present as thicker bundles and are comprised of longer filaments in the G2/M stage of the cell cycle (47). We therefore tested for actin cable assembly in yeast metaphase extracts. The yeast cell cycle is regulated by the periodic appearance of distinct cyclins, which activate cyclin-dependent kinase 1 (Cdk1) (48). We avoided the use of temperature-sensitive cell-cycle mutants to minimize potential heat shock effects on F-actin behavior (49). Instead, we used either hydroxyurea (HU) or nocodazole to arrest cells before preparing the cytoplasmic extracts. Examination of the cyclin levels revealed that the extracts from the HU- and nocodazole-treated cells showed elevated mitotic cyclin (Clb2) levels relative to S- and G1-phase cyclins (Clb5, Clb3, and Cln2) (Fig. 1*B*) (48). Strikingly, when GST-Bni1 FH1-COOH beads were incubated in extracts from HU- and nocodazole-arrested cells, actin cables polymerized from the beads (Fig. 1*A*). To control for effects of residual chemicals in our assays, we supplemented different concentrations of HU or nocodazole in unsynchronized cell extracts. We tested HU at 0.15 M, 7.5 mM, and 0.375 mM and nocodazole at 15 μM, 0.75 μM, and 0.0375 μM. We did not observe F-actin assembly in response to any of these treatments. (Representative images are shown in Fig. S1*B*.) Beads coated with GST alone were not sufficient to assemble actin filaments (Fig. S1*C*). In addition, we tested whether the other budding yeast formin, Bnr1, can assemble actin cables in the extract system. However, even though GST-Bnr1 FH1-COOH had a higher activity than GST-Bni1 FH1-COOH for pyrene actin nucleation in a solution assay (Fig. S1 *D* and *E*) (50), GST-Bni1 FH1-COOH on beads incubated in extracts from HU-arrested cells or in solutions of pure actin can nucleate actin cables, but GST-Bnr1 FH1-COOH cannot (Fig. S1 *F* and *G*).

Using extracts from HU- and nocodazole-arrested cells, 81.6 ± 8.7% and 80.3 ± 7.8% of GST-Bni1 FH1-COOH–coated beads, respectively, were surrounded by actin cables (Fig. 1*C*). The actin cables assembled at a rate of 2.9 ± 0.661 μm/min, which is equivalent to ∼18 subunits/s based on 370 subunits/μm of actin filament (Fig. S1*H*). This rate is of the same order of magnitude as actin cable assembly observed for budding yeast in vivo (51, 52). Once formed, the actin cables persisted for longer than 1 h.

To explore further the cell-cycle regulation of actin assembly, we performed the actin cable reconstitution in cell extracts prepared from cells arrested in metaphase by transcriptional repression of the *CDC20* gene (53). The endogenous *CDC20* promoter was replaced by a methionine promoter, allowing *CDC20* expression to be turned off upon addition of methionine-supplemented medium. Similar to extracts prepared from HU- and nocodazole-treated cells, extracts from *pMET-CDC20* arrested cells also initiated actin cable formation on Bni1 FH1-COOH–coated beads (Fig. 1 *A* and *C*).

To analyze the relationship between cable-assembly activity and cyclin expression, we synchronized *cdc15-2* cells expressing epitope tagged-cyclins (Table S1) and Abp140-3×GFP. *cdc15-2*

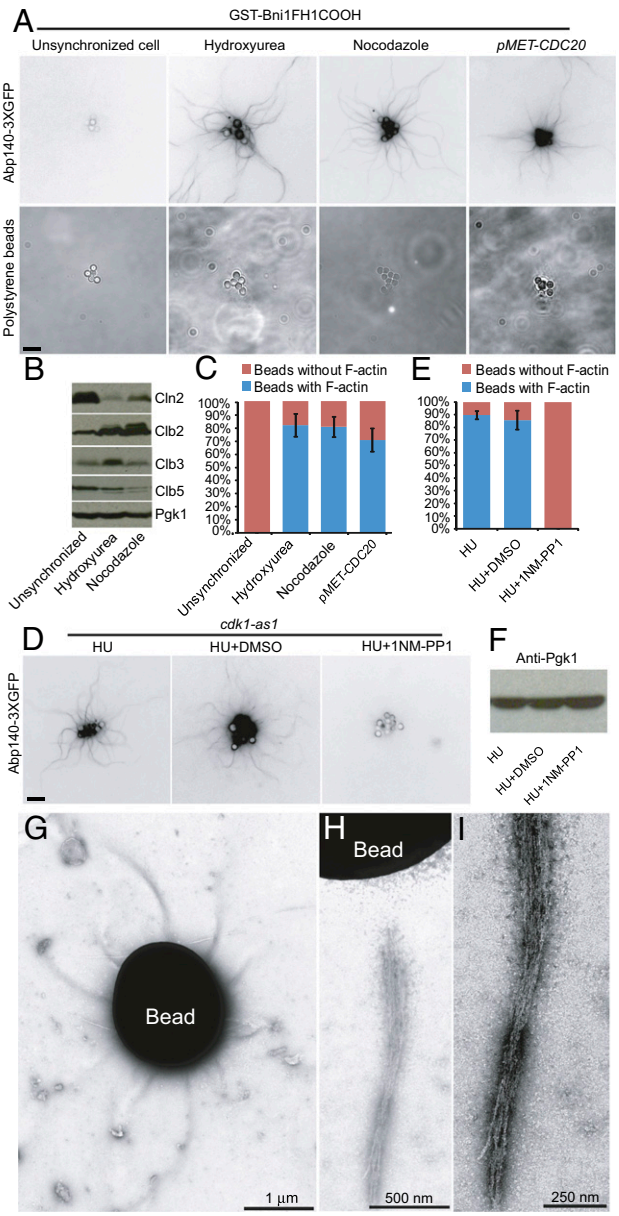

Fig. 1. Reconstitution of actin cables nucleated by Bni1 on polystyrene microspheres in yeast cytoplasmic extracts. (*A*) GST-Bni1 FH1-COOH–functionalized 2-μm microspheres were added to different cytoplasmic extracts generated from yeast cells expressing Abp140-3×GFP. Extracts prepared from HU-, nocodazole-, and *pMET*-CDC20–arrested cells, but not from unsynchronized cells, support actin cable assembly. Polystyrene beads are shown by transillumination. (*B*) The percentage of beads with or without actin cables for the reactions in *A*, including unsynchronized (n = 10 individual experiments) and HU- (n = 9), nocodazole- (n = 4), and *pMET*-CDC20–arrested cells (n = 4). (*C*) Cyclin levels were determined by Western blotting of extracts from unsynchronized and HU- and nocodazole-arrested cells. Pgk1 was used as a loading control. (*D*) Inhibition of Cdk1 activity using 1NM-PP1 on HU-arrested *cdk1-as1* cells before extract preparation blocks actin cable formation by GST-Bni1 FH1-COOH–coated beads. 1NM-PP1 at a final concentration of 20 μM was added for 30 min before sample preparation. (*E*) The percentage of beads with or without actin cables for reactions in *D* (n = 3). (*F*) The protein concentrations for cytoplasmic extracts used for actin reconstitution in *D* are compared by anti-Pgk1 Western blot. (Scale bars, 5 μm.) (*G–I*) Actin cables were assembled from GST-Bni1 FH1-COOH–functionalized beads in cell extracts derived from HU-arrested cells. Polymerized F-actin was negatively stained and visualized by EM. (*G*) Actin cables emanating from polystyrene beads, viewed at low magnification by negative-staining EM. (*H* and *I*) High-magnification images showing actin filament bundles.

cells were first arrested at late anaphase/telophase by incubation at 37 °C for 180 min (54). Then they were released by shifting to 25 °C, and cells were harvested every 30 min for parallel immunoblotting and actin cable-assembly assay. These studies revealed that the mitotic cyclin Clb2 is highly enriched in the extracts producing robust actin cable formation from GST-Bni1 FH1-COOH–functionalized beads (Fig. S2). However, the percentage of beads containing actin cables was lower (42%) than in extracts made from HU- or nocodazole-arrested cells. The most plausible explanation for the lower assembly in *cdc15* mutant extracts is that the temperature-sensitive mutant is not fully reversible.

We next tested whether Cdk1 kinase activity is required for actin cable assembly from Bni1 FH1-COOH beads. To address this question, endogenous Cdk1 was replaced by an analog-sensitive allele of Cdk1 (*cdk1-as1*), which can be specifically inhibited by the ATP analog 1-NM-PP1 (55-57). *cdk1-as1* cells were synchronized by HU addition and then were treated with 20 μM of the ATP analog 1-NM-PP1 for 30 min to inhibit the Cdk1 kinase activity specifically or as a control were treated with DMSO before extract preparation. Inhibition of Cdk1 activity caused actin cable-assembly activity to be abolished completely (Fig. 1 *D* and *E*), whereas treatment of Cdk1 WT cells with 1-NM-PP1 did not affect actin assembly (Fig. S1*I*). The loss of cable-assembly activity in inhibitor-treated *cdk1-as1* cells was not caused by a difference in soluble protein levels in the cytoplasmic extract, as shown by a phosphoglycerate kinase 1 (Pgk1) loading control (Fig. 1*F*).

Reconstituted Actin Cables Are Bundles of Actin Filaments. In yeast, actin cables are nucleated by formin proteins, stabilized by tropomyosin (Tpm1), are composed of bundles of short filaments, and are localized near the cell cortex (50, 52, 58–63). To analyze the structural properties of the actin structures nucleated from the Bni1 FH1-COOH beads in cytoplasmic extracts, we examined the reconstituted F-actin structures by negative-staining EM (Fig. 1 *G*–*I*). Actin filaments were assembled for 30 min on GST-Bni1 FH1-COOH beads and were subjected to negative staining on carbon-coated grids. Because of the high electron density of negatively stained polystyrene beads, a dark blurry area occupied a 200- to 300-nm zone around the beads. The actin filaments assembled from the GST-Bni1 FH1-COOH–coated beads appeared in EM as bundles comprised of 10-nm unbranched filaments with an average thickness of 83.8 ± 18.5 nm ($n = 52$ from 16 bundles, measured within 1 μm from the bead boundary). This dimension is consistent with the reported in vivo cable thickness (90–100 nm) at the G2/M stage in fission yeast (47). Because it was difficult to discern the ends of filaments, we could not calculate their individual lengths. Because Bni1 has not been reported to have a bundling activity (50), the appearance of bundles in the cytoplasmic extracts suggests the presence of bundling factors.

Recapitulation of Regulatory Protein Dependence During Actin Cable Reconstitution. To test how faithfully the Bni1 FH1-COOH–dependent actin cable-reconstitution system recapitulates the in vivo function of actin-regulatory proteins, we generated extracts from four mutants in which actin-interacting proteins were knocked out or rendered dysfunctional. These included the actin cable-specific stabilizing protein Tpm1, the barbed end-capping pro tein (Cap2), the depolymerization factor cofilin (Cof1), and the actin cable regulator Bud6. HU-arrested cells expressing Abp140-3×GFP were used for actin cable-reconstitution assays.

Mutants of different actin-interacting proteins showed distinct actin cable phenotypes (Fig. 2 *A*–*E*). Deletion of *TPM1* completely abolished cable formation (Fig. 2*B*), similar to the in vivo phenotype (58, 61). In contrast, cables formed in *cap2Δ* extracts were more numerous (>2.5 fold) than in WT extracts (Fig. 2 *F* and *H*), whereas aberrantly long actin cables were formed in cytoplasmic extracts from *cof1-4* mutant cells (Fig. 2*G*). These results are consistent with the observations that capping protein antagonizes formin activity and that cofilin promotes cable turnover in vivo (64–67). Addition of 5 μM Latrunculin A (LatA) to WT extracts subsequent to cable assembly caused complete actin cable disassembly within 5 min (Fig. S3 *A* and *C*), suggesting that assembled F-actin turns over dynamically in this extract system, similar to observations in live cells (52, 68, 69). In *cof1-4* extracts, however, reconstituted cables disassembled more slowly upon LatA addition (Fig. S3 *B* and *D*). Compared with WT extracts, *bud6Δ* extracts did not show obvious defects in actin cable assembly from beads (Fig. 2*E*). We found that our membrane-free cytoplasmic extract supernatants contain much less Bud6 than whole-cell extracts (Fig. S3*E*), which is consistent with the membrane-associated nature of Bud6 (70). Thus it is unlikely that the reason no effect on actin cable assembly was observed in *bud6Δ* extracts relative to WT extracts is because Bud6 levels are depleted in our WT extracts. The actin elongation rate in *bud6Δ* extracts also was similar to that in WT extracts (17 versus 18 subunits/s) (Fig. S3*F*). We found that actin polymerization is initiated with similar timing in WT and *bud6Δ* extracts and that the cables showed similar geometry (Fig. S3*G*). Taken together, these observations indicate that the Bni1 FH1-COOH–based actin cable-reconstitution system faithfully recapitulates the functions of actin-interacting proteins and actin cable dynamics and provides functional insights; therefore Bni1 FH1-COOH–based actin cable-reconstitution is a robust system for studies of actin cable assembly.

MS Reveals the Protein Composition of Bni1-Nucleated Actin Cables. To identify the proteins associated with the Bni1-derived actin cables, we performed MS on the F-actin structures assembled from beads in yeast extracts. We avoided using the F-actin–stabilizing drug phalloidin, which competes with some actin-binding proteins (71). Polystyrene beads with assembled actin cables were washed and prepared for MS (*Materials and Methods*). The MS analysis identified 592 yeast proteins (Dataset S1) using stringent criteria with false-discovery rates reduced to 0–0.5% (*Materials and Methods*). Because of the high sensitivity of MS identification, we used a statistical method to identify the enriched proteins by comparing our MS results with the PeptideAtlas database using protein spectrum counts, as described previously (*Materials and Methods*) (24). Using this strategy, 115 proteins (Fig. 3 and Datasets S2 and S3) were found to be enriched in the Bni1 FH1-COOH–derived actin cables ($P < 0.05$). We normalized protein extract samples by loading equal protein in each lane (Fig. 3 *B* and *C*) and found that yeast actin was the most highly enriched and abundant protein (Fig. 3 *B* and *C*). The reconstituted cables also were enriched for the actin cytoskeleton proteins, fimbrin (Sac6), and Tpm1 (Fig. 3*D*), which associate with actin cables in vivo. Pgk1, a cytosolic 3-phosphoglycerate kinase with no known affinity for actin, was not detected (Fig. 3*C*).

Previously, we found that actin networks nucleated in yeast extracts by the Arp2/3 complex consisted largely of proteins associated with Arp2/3-nucleated networks in cells (24). Here, we detected actin-binding protein 1 (Abp1), thought to associate primarily with Arp2/3-derived actin patches, associated with Bni1 FH1-COOH–derived actin cables (Fig. 3*C*). However, the enrichment of Abp1 was 10 times less than observed in our actin patch reconstitution (24). A null allele of *ABP1* did not affect the formation of GST-Bni1 FH1-COOH–derived actin cables (Fig. S4*A*). Arp2/3 proteins similarly were detected by MS (Fig. 3*A*), immunoblotting (Fig. 3*C*), and detection of fluorescently tagged proteins (Fig. S4*B*). However, we did not detect the Arp2/3 nucleation-promoting factors Myo3/5, Las17, or Pan1 by MS, Western blotting, or by detection of fluorescently tagged proteins (Fig. S4 *C* and *D*). To test further whether GST-Bni1 FH1-COOH–mediated

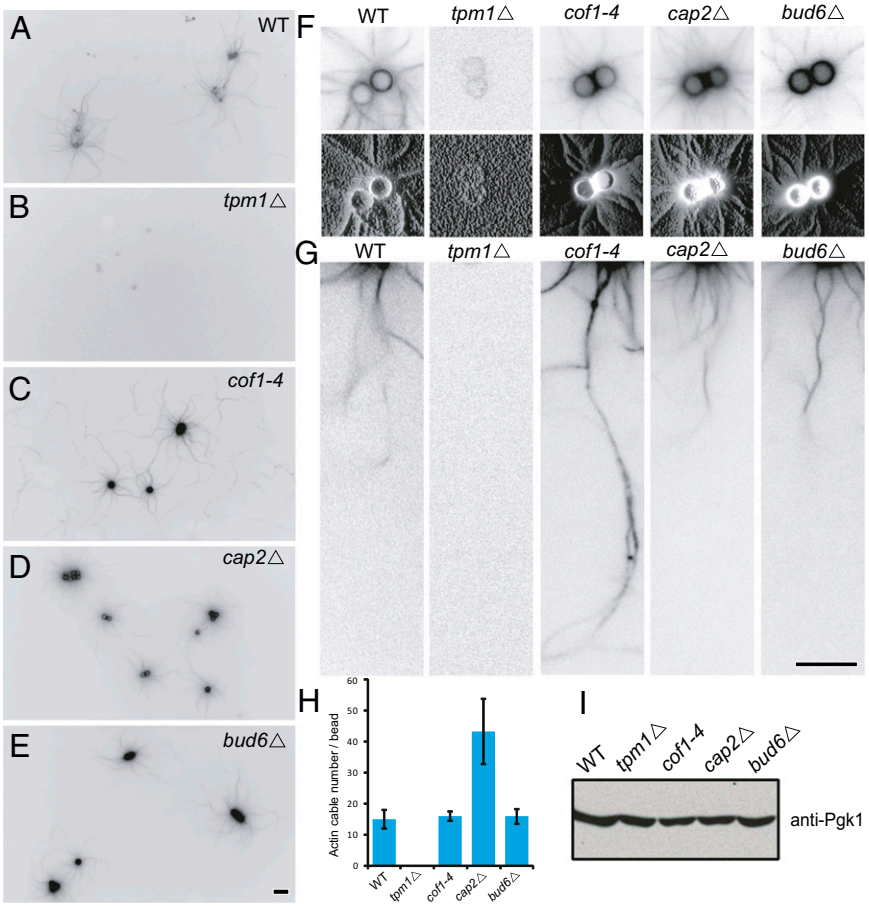

Fig. 2. Regulatory protein function tested in actin cable-reconstitution assay. GST-Bni1 FH1-COOH–functionalized beads were added to cytoplasmic extracts prepared from HU-arrested WT and *tpm1Δ*, *cap2Δ*, *cof1-4*, and *bud6Δ* cells expressing Abp140-3×GFP. (*A*–*E*) Actin cables assembled from GST-Bni1 FH1-COOH–functionalized beads during a 30-min incubation. (*F*) (*Upper*) Enlarged representative examples of actin cable reconstitution on beads incubated in extracts prepared from the indicated cell lines. (*Lower*) Actin cable patterns of upper panels are highlighted by 3D surface plots. (*Materials and Methods*). (*G*) Enlarged areas from *A*–*E* showing actin cables emanating from fluorescent beads. (*H*) Plot of number of actin cables per bead. Actin cable number was calculated based on the density of cables surrounding the bead at 0.25 μm away from the bead. (*I*) Control blot using anti-Pgk1 showing that similar cytoplasmic extract protein concentrations were used for actin cable reconstitutions in *A*–*E*. (Scale bars, 5 μm.)

actin cable assembly was dependent on Arp2/3 complex activity, we added the Arp2/3 complex inhibitor CK-666 and the control analog CK-689 at 100 μM to HU-arrested extracts. First, to test the activity and potency of the inhibitors, we used Las17-coated beads in HU extracts from cells expressing Abp1-mRFP. CK-666 at 100 μM, but not CK-689 or a DMSO control, effectively abolished actin tail formation, even though Abp1 still was recruited to the Las17-coated beads (Fig. S4*E*). However, CK-666 did not inhibit actin cable assembly from GST-Bni1 FH1-COOH–coated beads in HU-arrested extracts (Fig. S4 *F* and *G*) (72). Furthermore, although Bni1-derived actin filaments also form the contractile actomyosin ring in vivo (73), we did not detect the type II myosin Myo1 or the IQGAP protein Iqg1 by MS or by detection of fluorescently tagged proteins (Fig. 4*A* and Fig. S4*H*). These results suggest that the reconstituted actin structures primarily resemble actin cables rather than actin patches or the contractile ring.

Cdk1-Dependent Actin Cable Regulation in Vivo. To investigate how actin cables are regulated through the cell cycle in vivo, we first examined actin cables using super-resolution microscopy and Cdk1 inhibition using the *cdk1-as1* allele. We stained yeast actin filaments with Alexa-568 phalloidin in cells expressing GFP-tagged Tub1 (α-tubulin) (GFP-Tub1), an indicator of cell-cycle stage. To distinguish actin cables better, we resolved them by super-resolution 3D structured illumination microscopy (SIM), instead of by conventional fluorescence microscopy (Fig. 4*A* and Movie S1) (74). We measured the average signal intensity of actin cables in metaphase cells with high Cdk1 activity and in G1 cells with the lowest Cdk1 activity (75). We found that actin cables in metaphase cells had 21% higher average signal intensity than those in G1 cells, indicating that metaphase cells have a higher abundance of actin filaments per cable area than G1 cells (Fig. 4*B*). Second, we tested the effect of Cdk1 inhibition on actin cables in *bnr1Δ* cells that depend on Bni1 as the sole actin cable nucleator. We measured the speed of actin cable movement, a reflection of assembly rates, in living cells by following the positions of cable ends over time using Abp140-3×GFP. Because of the predominant cortical localization of cables (76), we monitored the actin cable movement close to cell cortex. In HU-arrested cells, actin cable ends moved at 1.18 ± 0.35 μm/s (Fig. 4*C*), similar to rates previously reported (76). However, when Cdk1 activity in *cdk1-as1* cells was inhibited by treatment with 20 μM 1-NM-PP1 for 30 min, actin cable velocity was reduced to 0.98 ± 0.23 μm/s (Fig. 4*C* and Movies S2 and S3). Finally, we examined the effects of Cdk1 inhibition on the average intensity of the actin cable signal by mixing Cdk1 and *cdk1-as1* cells in the same imaging sample to minimize sample-to-sample signal variation. To distinguish the two cell lines, Abp1-mRFP, which has a strong actin patch signal, and Bni1-3×mCherry, with a weak cortical signal, were used to distinguish

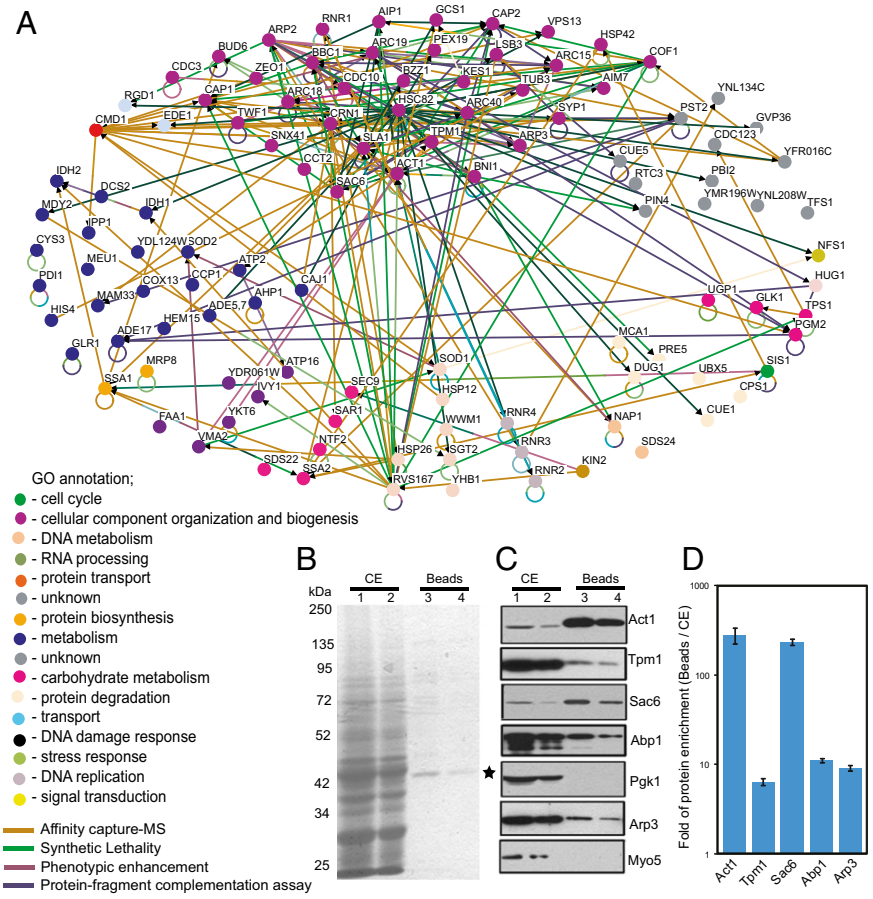

Fig. 3. Protein composition of formin-reconstituted actin cables. (*A*) Classification of actin cable components identified by MS with GO annotations. The Osprey-generated network displays published physical, genetic, and functional interactions based on the General Repository for Interaction Datasets. The key defines the dots and lines. (*B*) Coomassie blue-stained gel comparing composition of cell extracts (CE) with proteins associated with beads. Actin cables were polymerized on beads for 30 min in cytoplasmic extracts and then were subjected to washing and collection. Cell extract with 18.96 ± 1.72 μg soluble proteins (lane 1) can produce 0.44 ± 0.06 μg (lane 3) of actin cable-associated proteins on beads. Lanes 2 and 4 were loaded with half the amount of protein as lanes 1 and 3, respectively. The asterisk indicates actin. (*C*) Western blot of MS-identified proteins from reconstituted actin cables. Aliquots of samples used in *B* were resolved by SDS/PAGE, transferred to nitrocellulose, and probed by indicated antibodies. Note that mRFP antibody was used to detect Abp1 (Abp1-mRFP). (*D*) Quantification of *B* and *C*. The histogram shows the fold enrichment of the indicated proteins based on the amount of protein loaded (CE and Beads). Error bars with SD represent variability in measurements.

cdk1-as1 and Cdk1 WT cells, respectively. Cells first were arrested in HU for 3 h, followed by treatment for 30 min in DMSO alone as a control or 20 μM 1-NM-PP1. Cdk1 and *cdk1-as1* cells showed similar signal intensities upon DMSO treatment (Fig. 4*D*). However, the average actin cable signal was 40% lower in in *cdk1-as1* cells in which Cdk1 was inhibited by 1-NM-PP1 than in cells with normal Cdk1 activity (Fig. 4 *D* and *E*). To assess the specificity of this effect, we also tested whether Cdk1 activity is important for clathrin-mediated endocytosis, which is driven by Arp2/3-dependent actin filament nucleation. We did not observe detectable changes in the lifetimes or the dynamics of endocytic proteins of the early module (Ede1, Syp1), the coat module (Sla1), or the actin module (Abp1) upon inhibition of Cdk1 activity (Fig. S5) (77).

Cell-Cycle–Dependent Actin Cable Assembly Is Conserved in Vertebrates. The basic cell-cycle regulatory machinery consisting of Cdk1 and cyclins shows high conservation between yeast and vertebrate cells (48). To determine whether cell-cycle regulation of actin cable assembly is conserved from yeast to vertebrates, we performed actin cable-assembly reconstitutions in metaphase and interphase *Xenopus laevis* extracts, using the mammalian formin protein, mDia2. In mammalian cells, mDia2 plays an important role in generating actin filament bundles for filopodia protrusion (78–80). We coated polystyrene beads (2-μm diameter) with GST-mDia2 FH1-COOH and assayed for rhodamine-actin assembly in *Xenopus* extracts. Similar to our observations with GST-Bni1 FH1-COOH–coated beads in yeast extracts, GST-mDia2 FH1-COOH–coated beads nucleated actin filament assembly in metaphase *Xenopus* extracts (Fig. 5 *A* and *C*). Beads coated with GST alone did not nucleate actin filament assembly (Fig. S6 *A* and *D*). Moreover, actin filaments were not assembled from GST-mDia2 FH1-COOH–coated beads in interphase *Xenopus* extracts, although some actin filaments not associated with the beads were detectable in the background (Fig. 5 *B* and *D*). In addition, supplementation with 10 μM of the Cdk1 inhibitor RO-3306 completely abolished actin filament assembly from GST-mDia2 FH1-COOH–coated beads (Fig. S6 *B*, *C*, *E*, and *F*) (81). These observations demonstrate conservation of cell-cycle–regulated actin cable assembly.

Discussion

Yeast Actin Cable Reconstitution. We described here successful reconstitution of yeast actin cables in cell extracts using microbeads coated with the Bni1 FH1-COOH domain. This actin cable-reconstitution system recapitulates to a large degree the

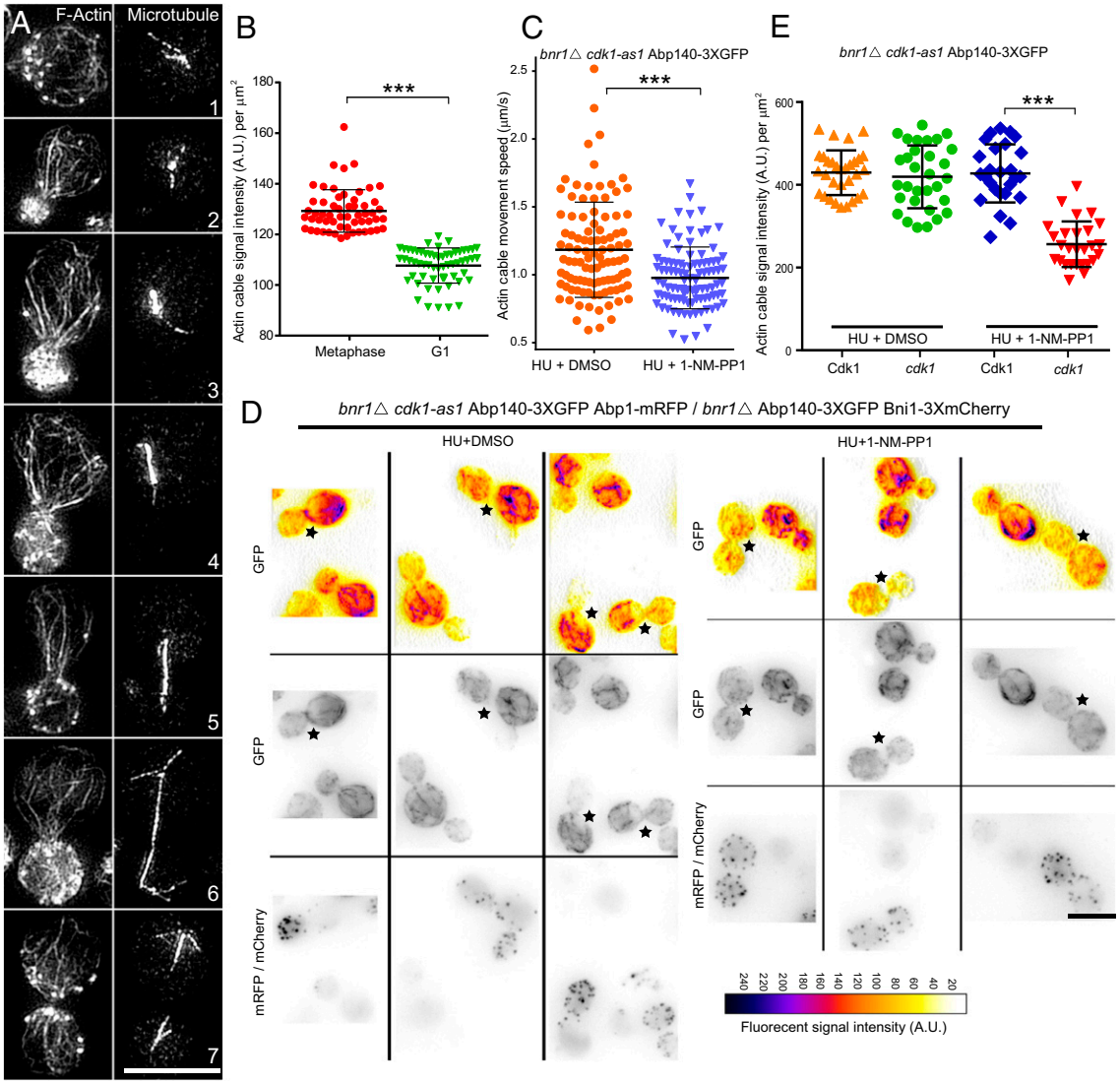

Fig. 4. In vivo Cdk1 regulation of formin-nucleated actin cables. (*A*) Average intensity projections along the *z*-axis of WT cells stained with Alexa-568 phalloidin to label actin filaments and expressing GFP-Tub1 as a cell-cycle stage indicator, obtained using 3D SIM microscopy. (Scale bar, 5 μm.) (*B*) Measurements of average signal intensity of actin cables (in arbitrary units, AU) per unit area (in square micrometers) in metaphase cells with spindle lengths of 1–2 μm ($n = 57$) (subpanels *3* and *4* in *A*) and G1-phase cells ($n = 58$) (subpanel *1* in *A*). (*C*) Measurements of the speed of actin cable movement in mother cells of *bnr1Δ cdk1-as1* with or without 1-NM-PP1 treatment. 1-NM-PP1 (20 μM) was applied to HU-arrested cells ($n = 100$) for 30 min. (*D*) Change in actin cable signal intensity by Cdk1 inhibition in HU-arrested *cdk1-as1 bnr1Δ* Abp140-3×GFP Abp1-mRFP and Cdk1 *bnr1Δ* Abp140-3×GFP Bni1-3XmCherry cells. (*Top*) Three-dimensional surface plots of actin cables have been assigned ImageJ Fire-LUT colors. Color key is shown at bottom. (*Middle*) Actin cables labeled by Abp140-3×GFP in cells with or without the *cdk1-as1* allele. (*Bottom*) Fluorescent signals from Abp1-mRFP or Bni1-3XmCherry in cells with or without the *cdk1-as1* allele, respectively. The stars indicate *cdk1-as1* cells. (Scale bar, 5 μm.) (*E*) Measurements of average signal intensity of actin cables in DMSO ($n = 31$) or HU-arrested cells with WT Cdk1 ($n = 26$) or the *cdk1-as1* mutant allele ($n = 27$) followed by treatment with 20 μM 1-NM-PP1 for 30 min. *P* values were determined by two-tailed Student *t* test assuming equal variances; $***P < 0.0001$.

properties observed for actin cables in vivo: (*i*) the cables consist of bundles of actin filaments; (*ii*) they contain biologically relevant cable-associated proteins; (*iii*) their assembly shows a dependence on the relevant actin-regulatory proteins; and (*iv*) the cables are under cell-cycle regulation. This reconstitution system also facilitated the identification of previously unknown actin cable components.

Understanding how Actin Cables of Defined Architecture and Protein Composition Assemble. In yeast cells, both branched endocytic actin networks and cables composed of unbranched actin filaments are assembled from the same actin but are nucleated by distinct factors, the Arp2/3 complex and formin proteins, respectively. How different actin-based structures with distinct associated proteins and distinct architectures are assembled in a common cytoplasm is an important unanswered question. Results here reinforce the conclusion that the identity of an actin filament is established upon its birth, likely mediated by the distinct nucleation factors, and is reinforced by competitive and cooperative interactions of proteins with actin filaments and by filament twist (1, 82).

The actin cable-reconstitution system enabled us to identify, in an unbiased manner using MS, factors involved actin cable formation. As with our previous actin patch reconstitution (1), MS was used to generate an actin cable parts list. This parts list in turn was used to identify candidate cable regulators, whose functions we tested using the reconstitution system and genetics.

The cable-associated proteins identified by MS included Bud6, a cofactor for Bni1 (46, 83); the barbed end-capping proteins Cap1/Cap2 (84, 85); the filament-stabilizing protein Tpm1 (58, 61); the filament-bundling protein Sac6 (86, 87); and the depolymerization factors Cof1, actin-interacting protein 1, coronin 1 (Crn1), and Srv2 (88–90).

Function of Actin-Binding Proteins in Actin Cable Assembly. The actin cable-reconstitution system allowed the functions of cable regulators to be tested in the context of the full complexity of the cytoplasm. The actin filament-stabilizing protein Tpm1 was enriched in the reconstituted cables, and actin cable assembly showed a pronounced dependence on Tpm1 that recapitulates the in vivo dependence (58, 61).

Sensitivity of the reconstituted actin cables to the actin inhibitor LatA established that the actin filaments in the cables turn over dynamically in the extract system. In vivo studies using LatA demonstrated that actin cable turnover depends on cofilin function in vivo (67). Cofilin has different activities on actin filaments in vitro, depending on the concentration (91), so it was important to test cofilin's cable-regulatory role in the context of the full complexity of the extract system. Cofilin does not localize to actin cables detectably in vivo except in an *aip1*-null mutant (64, 86, 92). In extracts prepared from a cofilin mutant, actin cables were clearly longer and less sensitive to LatA treatment, consistent with the in vivo observations (67).

The heterodimeric capping protein competes with formins for actin filament barbed ends in vitro (64–66). Our results with the reconstituted actin cables assembled in yeast extracts reinforced observations made with pure proteins in vitro. We found that more cables assembled in extracts deficient in capping protein.

We also found that proteins of the small heat shock protein family (sHsps) were enriched with the reconstituted actin cables. Three sHsp proteins—Hsp12, Hsp26, and Hsp42—were identified in the actin cable preparations. Hsp12 and Hsp26 were unique to Bni1-derived cables, but Hsp42 also was identified in association with Las17-derived actin patches (24). sHsps were reported to function as capping proteins or stabilization factors that protect actin filaments from severing proteins via direct or indirect interaction with actin filaments, indicating that functions for this family of proteins in cable regulation should be investigated further (93–96).

Cell-Cycle Regulation of Yeast Actin Cable Assembly. The yeast actin cytoskeleton undergoes a precise program of rearrangements throughout the cell cycle (97). The basis for these changes is not known, but we showed that inhibition of Cdk1 activity reduced cable-assembly rates and cable intensity in vivo. Recent reports in metazoans revealed up-regulation of actin assembly during metaphase (42, 43, 45). However, which types of actin filament networks are being regulated and which actin nucleation systems are being regulated are unclear. The Arp2/3 complex was suggested to be responsible for such metaphase-specific events for cell division (43, 45, 98). On the other hand, the formin protein Fmn2 was suggested to cooperate with Spire to assemble metaphase actin filaments for asymmetric cell divisions (99–101).

Here, we found that formin-mediated actin cable assembly was enhanced substantially in mitotic cell extracts in both yeast and vertebrates. Cdk1 activity was indispensible for reconstitution of yeast actin cable assembly, and the extracts that best supported cable assembly were enriched in the mitotic cyclin Clb2. Cdk1 activity also showed in vivo regulation of the speed of actin cable movement and cable intensity. No such effects were observed for Arp2/3-mediated actin nucleation, consistent with the observation that inhibition of Cdk1 activity did not affect endocytic internalization (102). In contrast to Bni1-derived actin cable reconstitution, Las17-derived actin networks can be reconstituted successfully in cytoplasmic extracts prepared from unsynchronized cells (24). Consistently, we did not observe detectable changes in the lifetimes or the dynamic behavior of endocytic patch proteins upon inhibition of Cdk1 activity in cells.

Presently, we do not know how many cable components are regulated by Cdk1 activity. In previous studies, several cable related proteins were identified as Cdk1 substrates in both in vivo and in vitro studies, and their phosphorylation levels were changed upon Cdk1 inhibition. These proteins include Bni1, Bud6, Crn1, Cap2, and Cof1 (55, 103). Bni1 and Bud6 might not be major determinants of cell-cycle–regulated actin cable assembly in our extracts, because we used constitutively active Bni1 and because Bud6 absence did not affect actin cable assembly. Interestingly, Cdk1 inhibition resulted in

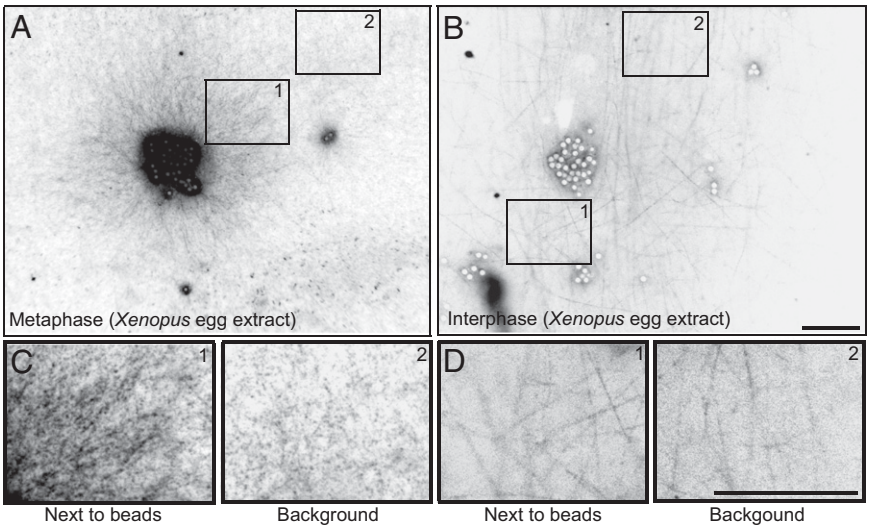

Fig. 5. Cell-cycle regulation of formin-nucleated actin assembly in vertebrate extracts. Polystyrene beads (2 μm) coated with GST-mDia2 FH1-COOH were added to metaphase (*A*) and interphase (*B*) *X. laevis* egg extracts. Then 0.4 μM of G-actin containing 20% Rhodamine-actin was added to the extracts. Images were taken after 30 min of incubation. *C* and *D* are magnified fields of *A* and *B*, respectively. The left subpanels in *C* and *D* show boxed area 1 (a field next to the beads) in *A* and *B*, respectively; the right subpanels in *C* and *D* show boxed area 2 (a field at least 15 μm away from the beads) in *A* and *B*, respectively. (Scale bars, 20 μm.)

Cof1 phosphorylation on Ser4 (55). A serine-to-alanine mutant on Ser4 of Cof1, *cof1-4*, shows aberrantly long cables in our extract assay. How Cdk1 affects Cof1 phosphorylation and the biological effects require further study. Furthermore, because we found that Cdk1 regulates actin cable intensity in vivo, bundling proteins should be investigated. The cell-cycle–dependent reconstitution of actin cable assembly in extracts from budding yeast, a favorite model for cell-cycle studies, opens the way toward elucidating the regulatory mechanism and identifying the relevant Cdk1 targets.

Materials and Methods

Yeast Strains, Growth Conditions, and Plasmids. Yeast strains used in this study are listed in Table S1. C-terminal GFP and RFP tags were integrated by homologous recombination, as described previously (77, 104). All strains were grown at 30 °C in standard rich medium (Yeast Extract Peptone Dextrose, YPD) or synthetic medium supplemented with appropriate amino acids, unless otherwise noted. Plates were incubated for 3 d before scoring cell growth.

Protein Purification. GST-Bni1 COOH and Las17 were expressed and purified essentially as previously described (105), except for the method for breaking the cells. Yeast cells used for protein purification were ground using a 6870 Freezer/Mill (SPEX SamplePrep, LLC) for six cycles consisting of 3 min of beating followed by 1 min of cooling. Protein concentrations were determined using the Gelcode blue staining reagent (Thermo Scientific) with BSA as a standard.

Actin Filament Polymerization on Beads in Cell Extracts. Two-micrometer nonfunctionalized polystyrene microspheres (Polybead Microsphere; Polysciences, Inc.) were incubated on ice with 100 nM GST-formin proteins in 25 μL of HK buffer [10 mM Hepes buffer (pH 7.8), 0.1 M KCl] for 40 min before BSA was added to a concentration of 1% and incubation for additional 15 min. Beads were washed two times by HK buffer containing 0.1% BSA, were stored in 25 μL of HK buffer, and were used within 8 h without significant loss of actin cable-assembly activity.

Unsynchronized yeast cells were collected from cultures grown at 30 °C in YPD to OD_{600} 0.8–1.0. HU and nocodazole arrests were achieved by adding drugs to cells at an OD_{600} of 0.7 followed by culture for two additional generations. The drug concentrations used were 0.15 M for HU and 15 μM for nocodazole. To arrest cells carrying *pMET*-CDC20, methionine was added to a final concentration of 10 mM to cells at an OD_{600} of 0.7, followed by incubation at 30 °C for 3 h before collection. Cells were harvested by centrifugation at 3,000 × *g* for 10 min at 4 °C, were washed once in cold water, and were centrifuged again. Cells were resuspended at 180 OD/mL in cold water before being flash-frozen in liquid N_2 and were ground by mortar and pestle for actin polymerization assays on beads. Yeast powder was mixed gently and thawed with 10× HK buffer and protease inhibitors (Protease Inhibitor Mixture Set IV; Calbiochem, Merck4Biosciences) and was centrifuged for 25 min at 350,000 × *g*. The supernatant under the lipid layer was collected and used within 3 h. For all actin-reconstitution experiments using yeast cell extracts, 1 μL of the functionalized microsphere beads was added to 19 μL of extract to induce formation of actin filaments.

Xenopus extracts from oocytes arrested at metaphase by cytostatic factor were prepared and provided by the R. Heald laboratory, University of California, Berkeley, CA. Cytochalasin D was omitted from all steps during preparation. Interphase extracts were prepared from *Xenopus* extracts by the addition of calcium at a final concentration 0.4 mM to crude cytostatic factor extracts followed by incubation at room temperature for 30 min. Polystyrene beads coated with GST-mDia2 FH1-COOH (1 μL) were incubated with 8 μL of extract and 1 μL of 3 μM rabbit actin [20% (mol/mol) rhodamine-actin].

Actin Cable-Like Structure Purification and Sample Preparation for MS. Actin cable-like structures were assembled around the polystyrene microspheres for 30 min at room temperature in 500 μL of extract. Beads were collected and washed essentially as previously described (24).

Data-dependent tandem MS analysis was performed with a LTQ-Orbitrap mass spectrometer (ThermoFisher). Full MS and tandem mass spectra were extracted from raw files, and the tandem mass spectra were searched against a *Saccharomyces cerevisiae* protein database (database released on December 16, 2005). To estimate peptide probabilities and false-discovery rates accurately, we used a reverse decoy database containing the reversed sequences of all the proteins appended to the target database (106). Tandem mass spectra were matched to sequences using the ProLuCID algorithm.

ProLuCID searches were done on an Intel Xeon 80 processor cluster running under the Linux operating system. The peptide mass search tolerance was set to 10 ppm for spectra acquired on the LTQ-Orbitrap instrument. The mass of the amino acid cysteine was statically modified by +57.02146 Da, to take into account the carboxyamidomethylation of the sample. No enzymatic cleavage conditions were imposed on the database search, so the search space included all candidate peptides whose theoretical mass fell within the mass tolerance window, regardless of their tryptic status (107, 108).

The validity of peptide/spectrum matches (PSMs) was assessed in DTASelect (109, 110) using two SEQUEST-defined parameters, the cross-correlation score (XCorr), and normalized difference in cross-correlation scores (DeltaCN). The search results were grouped by charge state (+1, +2, +3, and greater than +3) and tryptic status (fully tryptic, half-tryptic, and nontryptic), resulting in 12 distinct subgroups. In each of these subgroups, the distribution of Xcorr and DeltaCN values for (*i*) direct and (*ii*) decoy database PSMs was obtained; then the direct and decoy subsets were separated by discriminant analysis. Full separation of the direct and decoy PSM subsets generally is not possible; therefore, peptide match probabilities were calculated based on a nonparametric fit of the direct and decoy score distributions. A peptide probability of 90% was set as the minimum threshold. The false-discovery rate was calculated as the percentage of reverse decoy PSMs among all of the PSMs that passed the 90% probability threshold. In addition, we required that every protein be supported by at least a unique peptide with probability greater than 99%. After this last filtering step, we estimate that both the protein and peptide false-discovery rates were reduced to between 0.0 and 0.5%. (Dataset S1).

Because of the nature of the complex mixtures from cell extract samples, we took advantage of spectrum counting, which provides more reproducible linear correlations with protein abundance (24, 111, 112), to identify the enriched proteins in our reconstituted actin filament system. To analyze the peptide enrichment in specific protein samples, we compared the spectral counts of the actin assembly samples with spectral counts for peptides in PeptideAtlas (www.peptideatlas.org/) (113), which contains an inventory of 60,313 distinct peptides from *Saccharomyces cerevisiae* proteome (version Dec. 2011). By comparison with the PeptideAtlas database, the statistical significance for each protein (Dataset S2) from an actin assembly sample identified by LC-MS/MS was determined by calculating the one-sided *P* value of a Fisher's exact test with R (www.R-project.org/). Only six proteins identified in the actin assembly samples were not recorded in the PeptideAtlas database. We chose a P value < 0.05 as a threshold to identify the proteins enriched with the highest probability. Network diagrams for enriched proteins were generated by Osprey 1.0.1 (114) software by Gene Ontology (GO) annotation (The Gene Ontology Consortium, 2000; Dataset S3) derived from the *Saccharomyces* Genome Database (www.yeastgenome.org). Only interactions among indentified proteins were shown to reduce the complexity.

EM. Actin cables were reconstituted in 1.5-mL Eppendorf tubes by incubating GST-Bni1 FH1-COOH–coated beads with yeast extract for 30 min. Beads were collected and washed in HK buffer as previously described (24) and then were resupended in HK buffer, immediately spotted (10 μL) onto carbon-coated copper grids, and negatively stained with 2% (wt/vol) aqueous uranyl acetate for 2 min. Air-dried samples were examined at 120 kV in a Tecnai 12 transmission electron microscope (FEI), and images were recorded using an Ultrascan 1000 CCD camera (Gatan, Inc.).

Fluorescence Microscopy and Image Analysis. For the in vitro bead assay, 3.2 μL of cell extract containing functionalized beads was placed between a slide and a coverslip, which was sealed with a 1:1:1 mixture of Vaseline, lanolin, and paraffin. Bead assay images were acquired using an Olympus IX81 microscope equipped with a 60× PlanApo objective and a CCD camera (Orca II; Hamamatsu Photonics). For imaging yeast fluorescent signals in vivo, cells were immobilized as described previously (77, 104), and images were acquired using a Nikon Eclipse Ti-E inverted microscope (Nikon) with a solid-state Spectra-X light engine (Lumencor), a 100×/NA1.40 Plan Apo VC objective, and a Neo sCMOS camera (Andor Technology). Imaging data were collected using Metamorph software (Molecular Devices) and processed using Image J (National Institutes of Health). 3D SIM images were acquired essentially as previously described (115). The interactive 3D surface plot plugin of Image J was used for actin cable pattern demonstration by measuring the surface fluorescent signal intensity. The lifetimes of actin patches were measured by Imaris software (Bitplane Scientific) as previously described (116).

Western Blotting. Yeast whole-cell extracts were prepared as described previously (117). The following antibodies were used in this study: anti-myc antibody (1:5,000; 9E10), anti-RFP antibody (1:2,000; Rockland), anti-Pgk1 antibody (1:10,000; Invitrogen), anti-clb2 (y-180) (1:400; Santa Cruz Biotechnology), anti-clb3 (y-427) (1:400; Santa Cruz Biotechnology), anti-HA (12CA5) (1:5,000; Roche), anti-Sac6 (polyclonal) (1:2,000), anti-Tpm1 (polyclonal) (1:1,000), anti-Arp3 (yG-18) (1:250 Santa Cruz Biotechnology), and anti-Act1 (polyclonal) (1:2,000).

ACKNOWLEDGMENTS. We thank Derek McCusker for integrating the *cdk1-as1* allele into our DDY yeast strain background; David Kovar for mDia2 FH1-COOH protein; Qing Zhang for help with MS data analysis; the R. Heald laboratory for providing *Xenopus laevis* egg extracts; the Biological Imaging Facility for use of the Imaris software; and Christa Cortesio, Anthony Cormier, Yutian Peng, Jeffrey Woodruff, Derek McCusker, Charles Boone, and Michael Costanzo for helpful discussions and critical reading of the manuscript. Y.M. was supported by Human Frontier Science Program Fellowship LT000206/2010-L, and D.G.D. was supported by National Institutes of Health Grant R01 GM42759.

1. Michelot A, Drubin DG (2011) Building distinct actin filament networks in a common cytoplasm. *Curr Biol* 21(14):R560–R569.
2. Kaksonen M, Toret CP, Drubin DG (2006) Harnessing actin dynamics for clathrin-mediated endocytosis. *Nat Rev Mol Cell Biol* 7(6):404–414.
3. Pollard TD (2007) Regulation of actin filament assembly by Arp2/3 complex and formins. *Annu Rev Biophys Biomol Struct* 36:451–477.
4. Goley ED, Welch MD (2006) The ARP2/3 complex: An actin nucleator comes of age. *Nat Rev Mol Cell Biol* 7(10):713–726.
5. Pruyne D, et al. (2002) Role of formins in actin assembly: Nucleation and barbed-end association. *Science* 297(5581):612–615.
6. Evangelista M, Pruyne D, Amberg DC, Boone C, Bretscher A (2002) Formins direct Arp2/3-independent actin filament assembly to polarize cell growth in yeast. *Nat Cell Biol* 4(1):32–41.
7. Sagot I, Klee SK, Pellman D (2002) Yeast formins regulate cell polarity by controlling the assembly of actin cables. *Nat Cell Biol* 4(1):42–50.
8. Kovar DR, Harris ES, Mahaffy R, Higgs HN, Pollard TD (2006) Control of the assembly of ATP- and ADP-actin by formins and profilin. *Cell* 124(2):423–435.
9. Wu JQ, Pollard TD (2005) Counting cytokinesis proteins globally and locally in fission yeast. *Science* 310(5746):310–314.
10. Wu JQ, Kuhn JR, Kovar DR, Pollard TD (2003) Spatial and temporal pathway for assembly and constriction of the contractile ring in fission yeast cytokinesis. *Dev Cell* 5(5):723–734.
11. Evangelista M, et al. (1997) Bni1p, a yeast formin linking cdc42p and the actin cytoskeleton during polarized morphogenesis. *Science* 276(5309):118–122.
12. Yonetani A, Chang F (2010) Regulation of cytokinesis by the formin cdc12p. *Curr Biol* 20(6):561–566.
13. Basu R, Chang F (2007) Shaping the actin cytoskeleton using microtubule tips. *Curr Opin Cell Biol* 19(1):88–94.
14. Pelham RJ, Chang F (2002) Actin dynamics in the contractile ring during cytokinesis in fission yeast. *Nature* 419(6902):82–86.
15. Mooren OL, Galletta BJ, Cooper JA (2012) Roles for actin assembly in endocytosis. *Annu Rev Biochem* 81:661–686.
16. Akin O, Mullins RD (2008) Capping protein increases the rate of actin-based motility by promoting filament nucleation by the Arp2/3 complex. *Cell* 133(5):841–851.
17. Loisel TP, Boujemaa R, Pantaloni D, Carlier MF (1999) Reconstitution of actin-based motility of Listeria and Shigella using pure proteins. *Nature* 401(6753):613–616.
18. Upadhyaya A, van Oudenaarden A (2003) Biomimetic systems for studying actin-based motility. *Curr Biol* 13(18):R734–R744.
19. Wiesner S, et al. (2003) A biomimetic motility assay provides insight into the mechanism of actin-based motility. *J Cell Biol* 160(3):387–398.
20. Cameron LA, Footer MJ, van Oudenaarden A, Theriot JA (1999) Motility of ActA protein-coated microspheres driven by actin polymerization. *Proc Natl Acad Sci USA* 96(9):4908–4913.
21. Cameron LA, Robbins JR, Footer MJ, Theriot JA (2004) Biophysical parameters influence actin-based movement, trajectory, and initiation in a cell-free system. *Mol Biol Cell* 15(5):2312–2323.
22. Ho HY, et al. (2004) Toca-1 mediates Cdc42-dependent actin nucleation by activating the N-WASP-WIP complex. *Cell* 118(2):203–216.
23. Ma L, Cantley LC, Janmey PA, Kirschner MW (1998) Corequirement of specific phosphoinositides and small GTP-binding protein Cdc42 in inducing actin assembly in Xenopus egg extracts. *J Cell Biol* 140(5):1125–1136.
24. Michelot A, et al. (2010) Reconstitution and protein composition analysis of endocytic actin patches. *Curr Biol* 20(21):1890–1899.
25. Yarar D, To W, Abo A, Welch MD (1999) The Wiskott-Aldrich syndrome protein directs actin-based motility by stimulating actin nucleation with the Arp2/3 complex. *Curr Biol* 9(10):555–558.
26. Bernheim-Groswasser A, Wiesner S, Golsteyn RM, Carlier MF, Sykes C (2002) The dynamics of actin-based motility depend on surface parameters. *Nature* 417(6886):308–311.
27. McGrath JL, et al. (2003) The force-velocity relationship for the actin-based motility of Listeria monocytogenes. *Curr Biol* 13(4):329–332.
28. Suetsugu S, Miki H, Yamaguchi H, Takenawa T (2001) Requirement of the basic region of N-WASP/WAVE2 for actin-based motility. *Biochem Biophys Res Commun* 282(3):739–744.
29. Michelot A, et al. (2007) Actin-filament stochastic dynamics mediated by ADF/cofilin. *Curr Biol* 17(10):825–833.
30. Romero S, et al. (2004) Formin is a processive motor that requires profilin to accelerate actin assembly and associated ATP hydrolysis. *Cell* 119(3):419–429.
31. Alberts AS (2001) Identification of a carboxyl-terminal diaphanous-related formin homology protein autoregulatory domain. *J Biol Chem* 276(4):2824–2830.
32. Li F, Higgs HN (2005) Dissecting requirements for auto-inhibition of actin nucleation by the formin, mDia1. *J Biol Chem* 280(8):6986–6992.
33. Wallar BJ, et al. (2006) The basic region of the diaphanous-autoregulatory domain (DAD) is required for autoregulatory interactions with the diaphanous-related formin inhibitory domain. *J Biol Chem* 281(7):4300–4307.
34. Gould CJ, et al. (2011) The formin DAD domain plays dual roles in autoinhibition and actin nucleation. *Curr Biol* 21(5):384–390.
35. Copeland SJ, et al. (2007) The diaphanous inhibitory domain/diaphanous autoregulatory domain interaction is able to mediate heterodimerization between mDia1 and mDia2. *J Biol Chem* 282(41):30120–30130.
36. Seth A, Otomo C, Rosen MK (2006) Autoinhibition regulates cellular localization and actin assembly activity of the diaphanous-related formins FRLalpha and mDia1. *J Cell Biol* 174(5):701–713.
37. Lammers M, Rose R, Scrima A, Wittinghofer A (2005) The regulation of mDia1 by autoinhibition and its release by Rho*GTP. *EMBO J* 24(23):4176–4187.
38. Otomo T, Otomo C, Tomchick DR, Machius M, Rosen MK (2005) Structural basis of Rho GTPase-mediated activation of the formin mDia1. *Mol Cell* 18(3):273–281.
39. Li F, Higgs HN (2003) The mouse Formin mDia1 is a potent actin nucleation factor regulated by autoinhibition. *Curr Biol* 13(15):1335–1340.
40. Dong Y, Pruyne D, Bretscher A (2003) Formin-dependent actin assembly is regulated by distinct modes of Rho signaling in yeast. *J Cell Biol* 161(6):1081–1092.
41. Wang J, Neo SP, Cai M (2009) Regulation of the yeast formin Bni1p by the actin-regulating kinase Prk1p. *Traffic* 10(5):528–535.
42. Pinot M, et al. (2012) Confinement induces actin flow in a meiotic cytoplasm. *Proc Natl Acad Sci USA* 109(29):11705–11710.
43. Field CM, et al. (2011) Actin behavior in bulk cytoplasm is cell cycle regulated in early vertebrate embryos. *J Cell Sci* 124(Pt 12):2086–2095.
44. Chew TG, Lorthongpanich C, Ang WX, Knowles BB, Solter D (2012) Symmetric cell division of the mouse zygote requires an actin network. *Cytoskeleton, Hoboken* 69 (12):1040–1046.
45. Mitsushima M, et al. (2010) Revolving movement of a dynamic cluster of actin filaments during mitosis. *J Cell Biol* 191(3):453–462.
46. Moseley JB, et al. (2004) A conserved mechanism for Bni1- and mDia1-induced actin assembly and dual regulation of Bni1 by Bud6 and profilin. *Mol Biol Cell* 15(2): 896–907.
47. Kamasaki T, Arai R, Osumi M, Mabuchi I (2005) Directionality of F-actin cables changes during the fission yeast cell cycle. *Nat Cell Biol* 7(9):916–917.
48. Bloom J, Cross FR (2007) Multiple levels of cyclin specificity in cell-cycle control. *Nat Rev Mol Cell Biol* 8(2):149–160.
49. Ho J, Bretscher A (2001) Ras regulates the polarity of the yeast actin cytoskeleton through the stress response pathway. *Mol Biol Cell* 12(6):1541–1555.
50. Moseley JB, Goode BL (2005) Differential activities and regulation of Saccharomyces cerevisiae formin proteins Bni1 and Bnr1 by Bud6. *J Biol Chem* 280(30):28023–28033.
51. Huckaba TM, Lipkin T, Pon LA (2006) Roles of type II myosin and a tropomyosin isoform in retrograde actin flow in budding yeast. *J Cell Biol* 175(6):957–969.
52. Yang HC, Pon LA (2002) Actin cable dynamics in budding yeast. *Proc Natl Acad Sci USA* 99(2):751–756.
53. Uhlmann F, Wernic D, Poupart MA, Koonin EV, Nasmyth K (2000) Cleavage of cohesin by the CD clan protease separin triggers anaphase in yeast. *Cell* 103(3): 375–386.
54. Futcher B (1999) Cell cycle synchronization. *Methods Cell Sci* 21(2-3):79–86.
55. Holt LJ, et al. (2009) Global analysis of Cdk1 substrate phosphorylation sites provides insights into evolution. *Science* 325(5948):1682–1686.
56. Bishop AC, et al. (2000) A chemical switch for inhibitor-sensitive alleles of any protein kinase. *Nature* 407(6802):395–401.
57. Ubersax JA, et al. (2003) Targets of the cyclin-dependent kinase Cdk1. *Nature* 425(6960):859–864.
58. Liu HP, Bretscher A (1989) Disruption of the single tropomyosin gene in yeast results in the disappearance of actin cables from the cytoskeleton. *Cell* 57(2):233–242.
59. Buttery SM, Yoshida S, Pellman D (2007) Yeast formins Bni1 and Bnr1 utilize different modes of cortical interaction during the assembly of actin cables. *Mol Biol Cell* 18(5):1826–1838.
60. Sagot I, Rodal AA, Moseley J, Goode BL, Pellman D (2002) An actin nucleation mechanism mediated by Bni1 and profilin. *Nat Cell Biol* 4(8):626–631.
61. Drees B, Brown C, Barrell BG, Bretscher A (1995) Tropomyosin is essential in yeast, yet the TPM1 and TPM2 products perform distinct functions. *J Cell Biol* 128(3):383–392.
62. Goode BL, Eck MJ (2007) Mechanism and function of formins in the control of actin assembly. *Annu Rev Biochem* 76:593–627.
63. Karpova TS, McNally JG, Moltz SL, Cooper JA (1998) Assembly and function of the actin cytoskeleton of yeast: Relationships between cables and patches. *J Cell Biol* 142(6):1501–1517.
64. Harris ES, Li F, Higgs HN (2004) The mouse formin, FRLalpha, slows actin filament barbed end elongation, competes with capping protein, accelerates polymerization from monomers, and severs filaments. *J Biol Chem* 279(19):20076–20087.
65. Kovar DR, Wu JQ, Pollard TD (2005) Profilin-mediated competition between capping protein and formin Cdc12p during cytokinesis in fission yeast. *Mol Biol Cell* 16(5): 2313–2324.
66. Zigmond SH, et al. (2003) Formin leaky cap allows elongation in the presence of tight capping proteins. *Curr Biol* 13(20):1820–1823.
67. Okada K, Ravi H, Smith EM, Goode BL (2006) Aip1 and cofilin promote rapid turnover of yeast actin patches and cables: A coordinated mechanism for severing and capping filaments. *Mol Biol Cell* 17(7):2855–2868.

68. Ayscough KR, et al. (1997) High rates of actin filament turnover in budding yeast and roles for actin in establishment and maintenance of cell polarity revealed using the actin inhibitor latrunculin-A. *J Cell Biol* 137(2):399–416.
69. Cooper JA, Schafer DA (2000) Control of actin assembly and disassembly at filament ends. *Curr Opin Cell Biol* 12(1):97–103.
70. Jin H, Amberg DC (2000) The secretory pathway mediates localization of the cell polarity regulator Aip3p/Bud6p. *Mol Biol Cell* 11(2):647–661.
71. Nishida E, et al. (1987) Cofilin is a component of intranuclear and cytoplasmic actin rods induced in cultured cells. *Proc Natl Acad Sci USA* 84(15):5262–5266.
72. Nolen BJ, et al. (2009) Characterization of two classes of small molecule inhibitors of Arp2/3 complex. *Nature* 460(7258):1031–1034.
73. Vallen EA, Caviston J, Bi E (2000) Roles of Hof1p, Bni1p, Bnr1p, and myo1p in cytokinesis in Saccharomyces cerevisiae. *Mol Biol Cell* 11(2):593–611.
74. Gustafsson MG, et al. (2008) Three-dimensional resolution doubling in wide-field fluorescence microscopy by structured illumination. *Biophys J* 94(12):4957–4970.
75. Enserink JM, Kolodner RD (2010) An overview of Cdk1-controlled targets and processes. *Cell Div* 5:11.
76. Yu JH, Crevenna AH, Bettenbühl M, Freisinger T, Wedlich-Söldner R (2011) Cortical actin dynamics driven by formins and myosin V. *J Cell Sci* 124(Pt 9):1533–1541.
77. Kaksonen M, Toret CP, Drubin DG (2005) A modular design for the clathrin- and actin-mediated endocytosis machinery. *Cell* 123(2):305–320.
78. Mallavarapu A, Mitchison T (1999) Regulated actin cytoskeleton assembly at filopodium tips controls their extension and retraction. *J Cell Biol* 146(5):1097–1106.
79. Yang C, et al. (2007) Novel roles of formin mDia2 in lamellipodia and filopodia formation in motile cells. *PLoS Biol* 5(11):e317.
80. Block J, et al. (2008) Filopodia formation induced by active mDia2/Drf3. *J Microsc* 231(3):506–517.
81. Vassilev LT, et al. (2006) Selective small-molecule inhibitor reveals critical mitotic functions of human CDK1. *Proc Natl Acad Sci USA* 103(28):10660–10665.
82. Skau CT, Kovar DR (2010) Fimbrin and tropomyosin competition regulates endocytosis and cytokinesis kinetics in fission yeast. *Curr Biol* 20(16):1415–1422.
83. Graziano BR, et al. (2011) Mechanism and cellular function of Bud6 as an actin nucleation-promoting factor. *Mol Biol Cell* 22(21):4016–4028.
84. Wear MA, Cooper JA (2004) Capping protein: New insights into mechanism and regulation. *Trends Biochem Sci* 29(8):418–428.
85. Wear MA, Yamashita A, Kim K, Maéda Y, Cooper JA (2003) How capping protein binds the barbed end of the actin filament. *Curr Biol* 13(17):1531–1537.
86. Adams AE, Botstein D, Drubin DG (1989) A yeast actin-binding protein is encoded by SAC6, a gene found by suppression of an actin mutation. *Science* 243(4888):231–233.
87. Adams AE, Shen W, Lin CS, Leavitt J, Matsudaira P (1995) Isoform-specific complementation of the yeast sac6 null mutation by human fimbrin. *Mol Cell Biol* 15(1):69–75.
88. Chaudhry F, et al. (2013) Srv2/cyclase-associated protein forms hexameric shurikens that directly catalyze actin filament severing by cofilin. *Mol Biol Cell* 24(1):31–41.
89. Balcer HI, et al. (2003) Coordinated regulation of actin filament turnover by a high-molecular-weight Srv2/CAP complex, cofilin, profilin, and Aip1. *Curr Biol* 13(24):2159–2169.
90. Lin MC, Galletta BJ, Sept D, Cooper JA (2010) Overlapping and distinct functions for cofilin, coronin and Aip1 in actin dynamics in vivo. *J Cell Sci* 123(Pt 8):1329–1342.
91. Andrianantoandro E, Pollard TD (2006) Mechanism of actin filament turnover by severing and nucleation at different concentrations of ADF/cofilin. *Mol Cell* 24(1):13–23.
92. Rodal AA, Tetreault JW, Lappalainen P, Drubin DG, Amberg DC (1999) Aip1p interacts with cofilin to disassemble actin filaments. *J Cell Biol* 145(6):1251–1264.
93. Mounier N, Arrigo AP (2002) Actin cytoskeleton and small heat shock proteins: How do they interact? *Cell Stress Chaperones* 7(2):167–176.
94. Aufricht C, et al. (1998) Heat-shock protein 25 induction and redistribution during actin reorganization after renal ischemia. *Am J Physiol* 274(1 Pt 2):F215–F222.
95. Panasenko OO, Kim MV, Marston SB, Gusev NB (2003) Interaction of the small heat shock protein with molecular mass 25 kDa (hsp25) with actin. *Eur J Biochem* 270(5):892–901.
96. Miron T, Vancompernolle K, Vandekerckhove J, Wilchek M, Geiger B (1991) A 25-kD inhibitor of actin polymerization is a low molecular mass heat shock protein. *J Cell Biol* 114(2):255–261.
97. Lew DJ, Reed SI (1993) Morphogenesis in the yeast cell cycle: Regulation by Cdc28 and cyclins. *J Cell Biol* 120(6):1305–1320.
98. Yi K, et al. (2011) Dynamic maintenance of asymmetric meiotic spindle position through Arp2/3-complex-driven cytoplasmic streaming in mouse oocytes. *Nat Cell Biol* 13(10):1252–1258.
99. Leader B, et al. (2002) Formin-2, polyploidy, hypofertility and positioning of the meiotic spindle in mouse oocytes. *Nat Cell Biol* 4(12):921–928.
100. Pfender S, Kuznetsov V, Pleiser S, Kerkhoff E, Schuh M (2011) Spire-type actin nucleators cooperate with Formin-2 to drive asymmetric oocyte division. *Curr Biol* 21(11):955–960.
101. Schuh M, Ellenberg J (2008) A new model for asymmetric spindle positioning in mouse oocytes. *Curr Biol* 18(24):1986–1992.
102. McCusker D, Royou A, Velours C, Kellogg D (2012) Cdk1-dependent control of membrane-trafficking dynamics. *Mol Biol Cell* 23(17):3336–3347.
103. Loog M, Morgan DO (2005) Cyclin specificity in the phosphorylation of cyclin-dependent kinase substrates. *Nature* 434(7029):104–108.
104. Toshima JY, et al. (2006) Spatial dynamics of receptor-mediated endocytic trafficking in budding yeast revealed by using fluorescent alpha-factor derivatives. *Proc Natl Acad Sci USA* 103(15):5793–5798.
105. Rodal AA, Manning AL, Goode BL, Drubin DG (2003) Negative regulation of yeast WASp by two SH3 domain-containing proteins. *Curr Biol* 13(12):1000–1008.
106. Peng J, Elias JE, Thoreen CC, Licklider LJ, Gygi SP (2003) Evaluation of multidimensional chromatography coupled with tandem mass spectrometry (LC/LC-MS/MS) for large-scale protein analysis: The yeast proteome. *J Proteome Res* 2(1):43–50.
107. MacCoss MJ, et al. (2002) Shotgun identification of protein modifications from protein complexes and lens tissue. *Proc Natl Acad Sci USA* 99(12):7900–7905.
108. Lu B, Xu T, Park SK, Yates JR, 3rd (2009) Shotgun protein identification and quantification by mass spectrometry. *Methods Mol Biol* 564:261–288.
109. Cociorva D, Tabb D, Yates JR (2007) Validation of tandem mass spectrometry database search results using DTASelect. *Current Protocols in Bioinformatics* Chapter 13:Unit 13 14.
110. Tabb DL, McDonald WH, Yates JR, 3rd (2002) DTASelect and Contrast: Tools for assembling and comparing protein identifications from shotgun proteomics. *J Proteome Res* 1(1):21–26.
111. Zybailov B, Coleman MK, Florens L, Washburn MP (2005) Correlation of relative abundance ratios derived from peptide ion chromatograms and spectrum counting for quantitative proteomic analysis using stable isotope labeling. *Anal Chem* 77(19):6218–6224.
112. Liu H, Sadygov RG, Yates JR, 3rd (2004) A model for random sampling and estimation of relative protein abundance in shotgun proteomics. *Anal Chem* 76(14):4193–4201.
113. Deutsch EW, Lam H, Aebersold R (2008) PeptideAtlas: A resource for target selection for emerging targeted proteomics workflows. *EMBO Rep* 9(5):429–434.
114. Breitkreutz BJ, Stark C, Tyers M (2003) Osprey: A network visualization system. *Genome Biol* 4(3):R22.
115. Mennella V, et al. (2012) Subdiffraction-resolution fluorescence microscopy reveals a domain of the centrosome critical for pericentriolar material organization. *Nat Cell Biol* 14(11):1159–1168.
116. Doyon JB, et al. (2011) Rapid and efficient clathrin-mediated endocytosis revealed in genome-edited mammalian cells. *Nat Cell Biol* 13(3):331–337.
117. McCusker D, et al. (2007) Cdk1 coordinates cell-surface growth with the cell cycle. *Nat Cell Biol* 9(5):506–515.

Supporting Information

Miao et al. 10.1073/pnas.1314000110

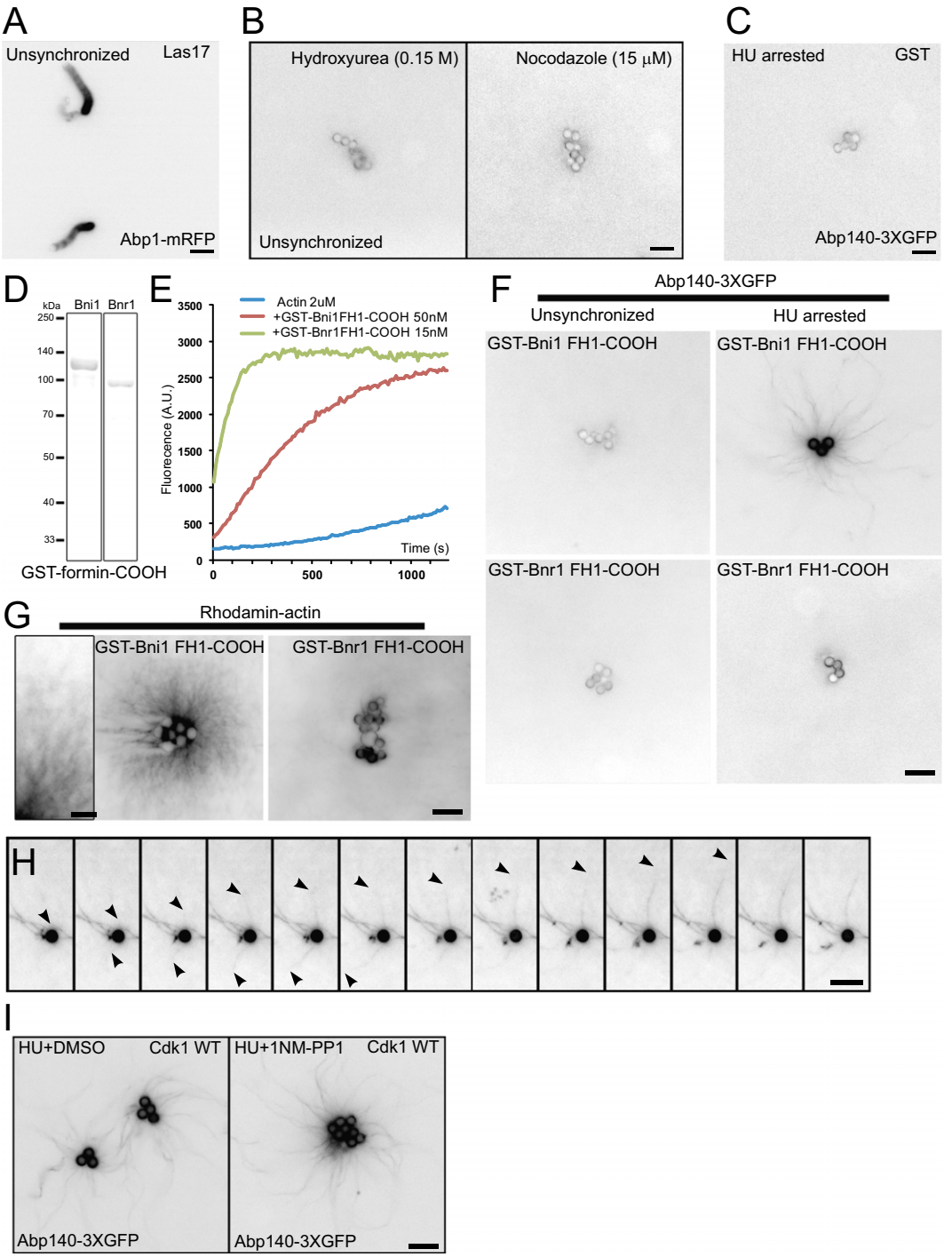

Fig. S1. GST-Bni1 FH1-COOH stimulated actin assembly. (*A*) Beads functionalized by incubation with 100 nM Las17 (yeast WASP) were incubated in a yeast cytoplasmic extract from unsynchronized cells. The image was taken after incubation for 1 h. (*B*) Reconstitution of actin cable assembly by Bni1-coated polystyrene microspheres in unsynchronized yeast extracts supplemented with 0.15 M hydroxyurea (HU) or 15 μM of nocodazole, respectively. (*C*) Beads coated by incubation in 100 nM GST were incubated in yeast cytoplasmic extract from HU-arrested cells. The image was taken after 30-min incubation. (*D*) Coomassie blue staining of GST-Bni1 FH1-COOH and GST-Bnr1 FH1-COOH purified from yeast. (*E*) Actin assembly kinetics: 2 μM monomeric actin [5% (mol/mol) pyrene-labeled] was assembled in the presence of the indicated concentrations of GST-Bni1 FH1-COOH and GST-Bnr1 FH1-COOH. (*F*) Beads functionalized by 100 nM of

Legend continued on following page

GST-Bni1 FH1-COOH or GST-Bnr1 FH1-COOH were incubated in yeast cytoplasmic extract from unsynchronized or HU-arrested cells. (*G*) Rabbit actin (1 μM) doped with 20% (mol/mol) Rhodamine-labeled rabbit actin was added to beads functionalized by 100 nM of GST-Bni1 FH1-COOH or GST-Bnr1 FH1-COOH. The image was taken after incubation of actin and beads for 15 min. (*Inset*) Higher-magnification view of actin filaments. (Scale bar in inset, 2 μm.). (*H*) Time course of actin filament assembly from the GST-Bni1 FH1-COOH–coated beads (30 s/frame) in extract from yeast arrested by HU. The rate of actin filament elongation (2.9 ± 0.661 μm/min) was measured by monitoring the ends of the elongating filaments (n = 21; representative images are shown). Arrowheads indicate the growing filament ends. (*I*) Treatment of HU-arrested cyclin-dependent kinase 1 (Cdk1) WT cells with 1NM-PP1 before extract preparation did not affect actin cable formation associated with GST-Bni1 FH1-COOH–coated beads. 1NM-PP1 at a final concentration of 20 μM was added for 30 min before cell harvesting. (Scale bars, 5 μm.)

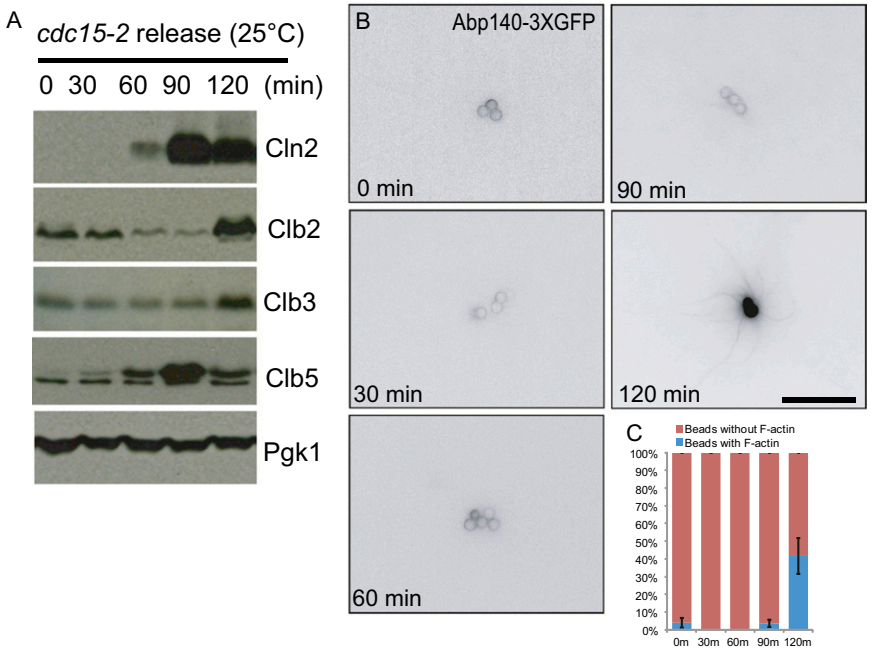

Fig. S2. Cell-cycle–dependent F-actin reconstitution by GST-Bni1 FH1-COOH. (*A*) The *cdc15-2* strain expressing Abp140-3×GFP was arrested at 37 °C for 3 h and then was released to 25 °C. Cells were collected at the indicated times after release and used for immunoblotting. Levels of cyclins Cln2, Clb2, Clb3 and Clb5 were determined. Phosphoglycerate kinase 1 (Pgk1) was used as a loading control. (*B*) Actin filament assembly was nucleated from GST-Bni1 FH1-COOH–coated beads using the cytoplasmic cell extracts described in *A*. (*C*) Quantitation of beads without or with F-actin assembly. Error bars indicate SD (n = 3 individual experiments). (Scale bar, 10 μm.)

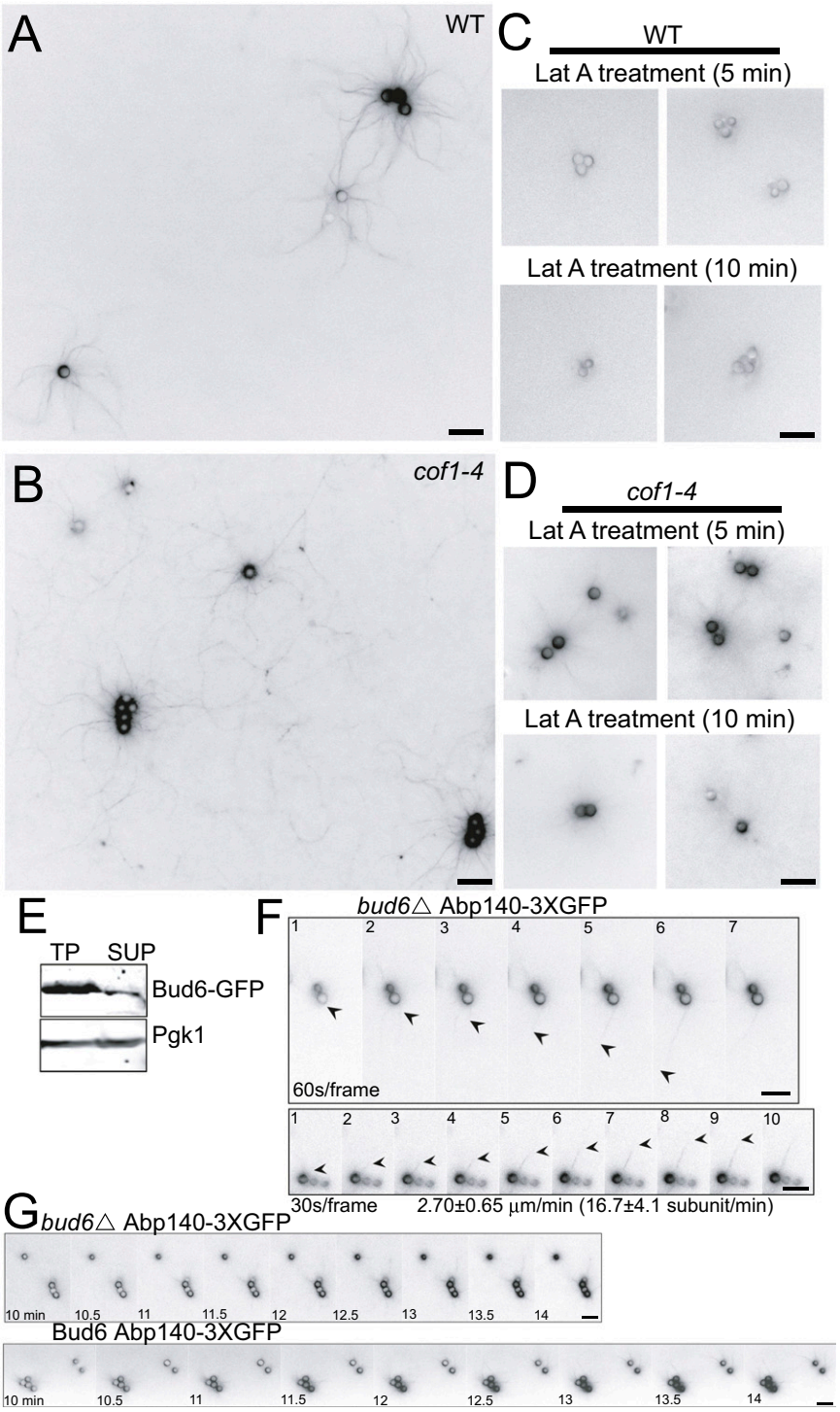

Fig. S3. Depolymerization of actin cables assembled in extracts. GST-Bni1 FH1-COOH–functionalized beads were added to cytoplasmic extracts prepared from HU-arrested WT and *cof1-4* cells expressing Abp140-3×GFP. (*A* and *B*) Actin cables assembled from GST-Bni1 FH1-COOH-functionalized beads during a 30-min incubation. (*C* and *D*) Latrunculin A (LatA) at final concentration of 5 μM was used to depolymerize actin cables in extracts. Images were taken at indicated times after LatA addition. (*E*) Bud site selector protein 6 (Bud6) distribution in yeast total protein (TP) and cytosolic supernatant (SUP) in extracts from a strain expressing Bud6-GFP. The cytosolic protein Pgk1 was used as a loading control. (*F*) Time course of actin filament assembly from the GST-Bni1 FH1-COOH–coated beads (*Upper*, 60s interval between frames; *Lower*, 30s interval between frames in an extract from *bud6Δ* cells arrested by HU. The rate of actin filament elongation (2.70 ± 0.65 μm/min) was measured by monitoring the ends of the elongating filaments (n = 49; representative images are shown). Arrowheads indicate the growing filament ends. (*G*) Initiation of actin filament assembly from the GST-Bni1 FH1-COOH–coated beads in HU extracts from *bud6Δ* and *BUD6* stains. (Scale bars, 5 μm.)

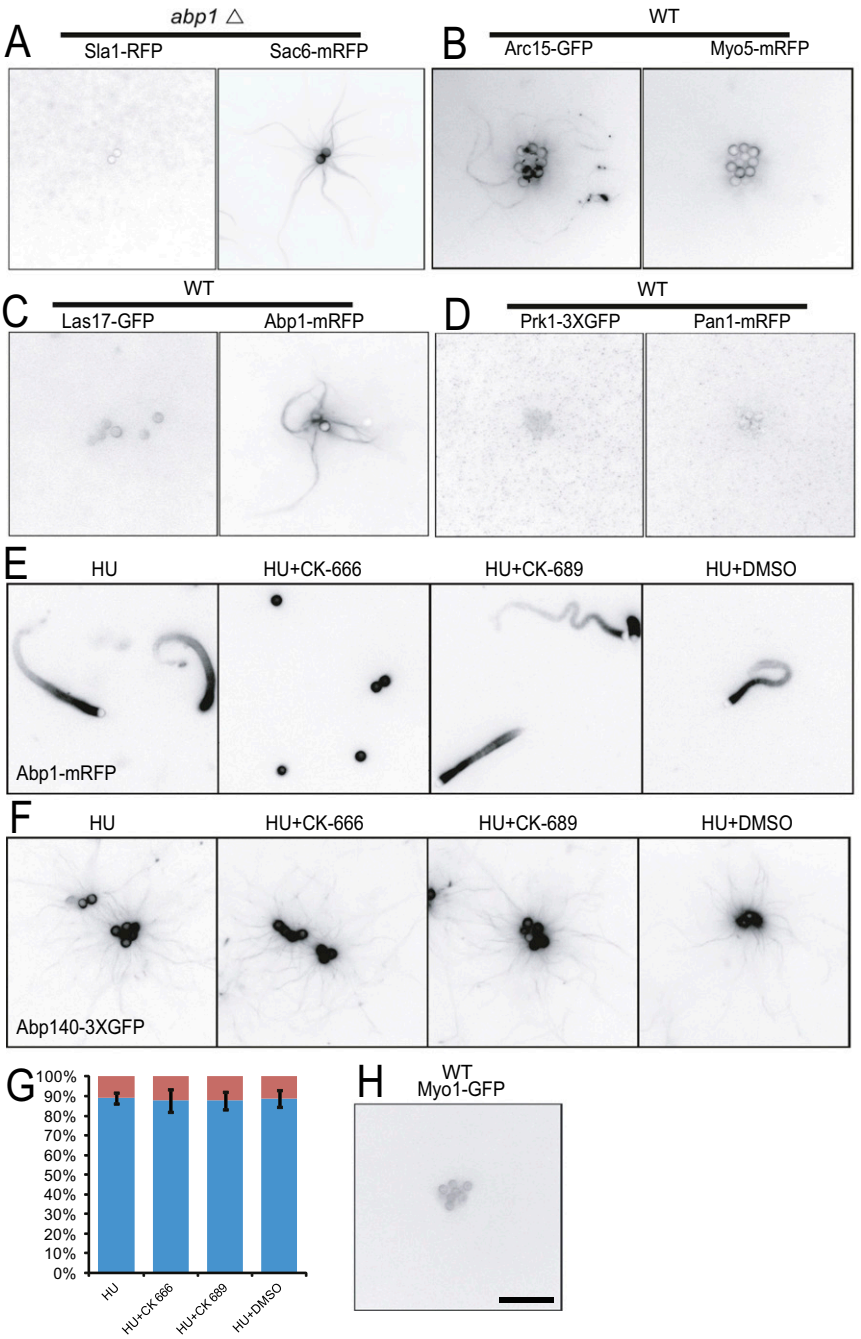

Fig. S4. Verification of association of protein components with reconstituted actin cables. (*A–D* and *H*) Yeast cells expressing indicated fluorescent fusion proteins were arrested by HU, extracts were prepared, and actin cables were reconstituted in the extracts on GST-Bni1 FH1-COOH–coated beads. Images were taken after 30 min of reaction. (*E*) The actin-related protein-2/3 (Arp2/3) inhibitor CK-666 inhibits actin tail formation from Las17-coated beads in yeast extract. CK-666 at 100 μM was added to HU-arrested extract containing beads coated with 100 nM Las17. The inactive analog CK-689 at 100 μM and DMSO were used as controls. (*F*) The Arp2/3 inhibitor CK-666 had no effect on actin cable assembly in yeast extract. CK-666 at 100 μM was added to an HU-arrested extract containing beads coated with 100 nM GST-Bni1 FH1COOH. Inactive analog CK-689 at 100 μM and DMSO were used as controls. Images were taken after 30 min of incubation. (*G*) The percentage of beads with or without actin cables for reactions in *F*. Error bars indicate SD ($n = 3$ individual experiments). (Scale bar, 10 μm.)

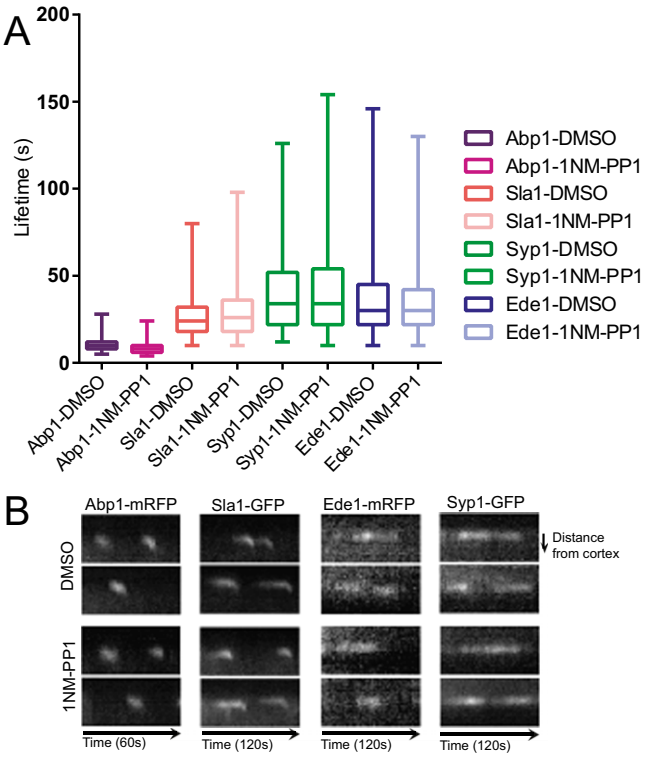

Fig. S5. Cdk1 activity is not required for endocytosis. (*A*) Patch lifetimes of Abp1-mRFP, Sla1-GFP, Ede1-GFP, and Syp1-GFP were measured in *cdk1-as1* cells that first were treated with 20 μM 1NM-PP1 or DMSO as a control for 30 min. Patch numbers used for calculations, from left to right: $n = 759$, $n = 1,046$, $n = 1,089$, $n = 2,103$, $n = 610$, $n = 1,199$, $n = 433$, and $n = 654$. Error bars indicate SD. The frame rate was one frame/s for Abp1-mRFP and one frame/2 s for Sla1-GFP, Ede1-GFP, and Syp1-GFP. (*B*) Kymographs of representative Abp1-mRFP, Sla1-GFP, Ede1-GFP, and Syp1-GFP patches from epifluorescence movies of *cdk1-as1* cells treated with 1NM-PP1 or DMSO (strains and treatment conditions are listed in *A*).

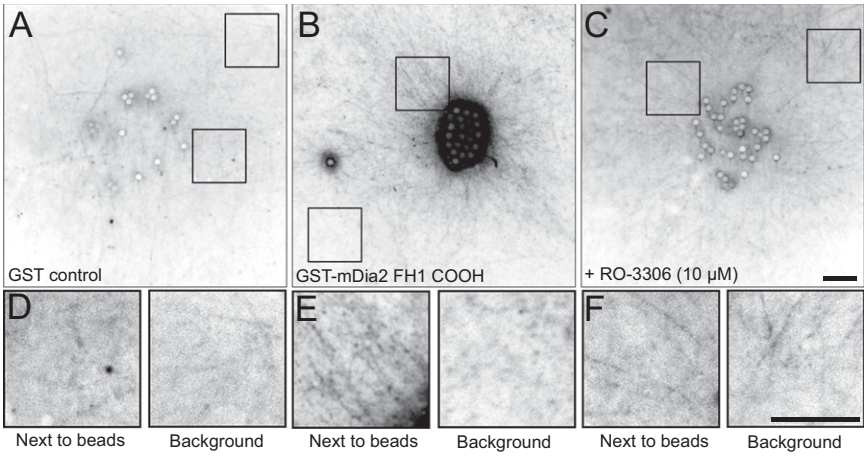

Fig. S6. Cdk1 activity is required for F-actin assembly in vertebrate extracts. Beads coated with GST (*A*) or GST-mDia2FH1-COOH (*B* and *C*) from 100-nM solutions were added to metaphase *Xenopus laevis* egg extracts. Extracts were preincubated with DMSO control (*B*) or 10 μM Cdk1 inhibitor RO-3306 (*C*) for 15 min at 25 °C before beads were added. Then 0.4 μM of rabbit G-actin containing 20% Rhodamine-actin was added to the extracts. Images were taken after 30 min of incubation. *D*–*F* are magnified fields of boxed areas in *A*–*C*, respectively. (Scale bars, 10 μm.)

Table S1. Strains used in this study

Strain	Genotype
DDY1102	*MATa/MATα his3-Δ200/his3-Δ200 ura3-52/ura3-52 leu2-3,112/leu2-3,112 lys2-801/LYS2 ade2-1/ADE2*
DDY904	*MATα his3-Δ200 leu2-3, 112, ura3-52*
DDY3074	*MATα his3-Δ200 leu2-3, 112, ura3-52 SLA1-GFP::KanMX6 SAC6-mRFP:HIS3 abp1Δ::CgLEU2*
DDY3276	*MATa his3-Δ200 ura3-52 leu2-3,112 lys2-801 ARC15-GFP::HIS3 MYO5-mRFP::HIS3*
DDY3111	*MATα his3-Δ200 ura3-52 leu2-3,112 lys2-801 LAS17-GFP::HIS3 ABP1-mRFP::HIS3*
DDY2065	*MATa his3-Δ200 ura3-52 leu2-3,112 lys2-801 pfy1-4::cgLEU2 act1-157::cgHIS3*
DDY4350	*MATα his3-Δ200 leu2-3, 112, ura3-52 ABP140*-3×GFP*::HIS3*
DDY4351	*MATα his3-Δ200 ura3-52 leu2-3,112 lys2-801 PRK1*-3×GFP*::URA3 PAN1-mRFP::HIS3*
DDY4352	*MATα his3-Δ200 leu2-3, 112, ura3-52 tpm1Δ::CgHIS3 ABP140*-3×GFP*::CgHIS3*
DDY4353	*MATα his3-Δ200 leu2-3, 112, ura3-52 cap2Δ::CgLEU2 ABP1-mRFP::HIS3 ABP140*-3×GFP*::HIS3*
DDY4354	*MATα his3-Δ200 leu2-3, 112, ura3-52 cof1-4::CgLEU2 ABP1-mRFP::HIS3 ABP140*-3×GFP*::HIS3*
DDY4355	*MATa his3-Δ200 leu2-3, 112, ura3-52 bud6Δ::cgURA ABP1-mRFP::HIS ABP140*-3×GFP*::HIS3*
DDY4356	*MATα his3-Δ200 leu2-3, 112, ura3-52 MYO1-GFP::HIS*
DDY4357	*MATα his3-Δ200 leu2-3, 112, ura3-52 cdk1-as1:NAT ABP1-mRFP::HIS3 ABP140*-3×GFP*::HIS3*
DDY4358	*MATα his3-Δ200 leu2-3, 112, ura3-52 cdk1-as1:NAT bnr1Δ::KanMX6 ABP1-mRFP::HIS3 ABP140*-3×GFP*::HIS3*
DDY4359	*MATα his3-Δ200 leu2-3, 112, ura3-52 CDK1:NAT bnr1Δ::KanMX6 BNI1-3XmCherry::HIS3 ABP140*-3×GFP*::HIS3*
DDY4360	*MATα his3-Δ200 leu2-3, 112, ura3-52 cdk1-as1:NAT ABP1-mRFP::HIS3 SLA1-GFP::HygMX6*
DDY4361	*MATα his3-Δ200 leu2-3, 112, ura3-52 cdk1-as1:NAT EDE1-mRFP::HIS3 SYP1-GFP::KanMX6*
DDY4406	*MATα his3-Δ200 leu2-3, 112, ura3-52 cdc15-2 CLN2-13XMYC::HIS3 ABP1-mRFP::HIS3 ABP140-3XGFP::HIS3 CLB5-3XHA::KanMX6*

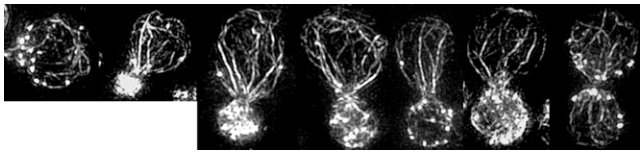

Movie S1. F-actin structures revealed by 3D structured illumination microscopy. Alexa-568 phalloidin were used to stain F-actin in budding yeast cells. 3D projections were created using ImageJ.

Movie S1

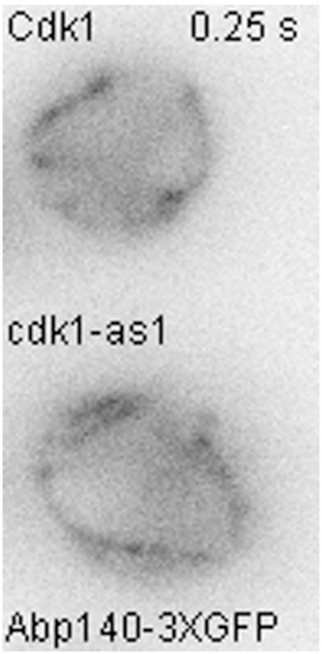

Movie S2. In vivo actin cable dynamics. The actin cable-assembly rate was assessed by imaging Abp140-3×GFP at the cortex of mother cells of *CDK1 bnr1Δ* Abp140-3×GFP Bni1-3XmCherry (*Upper*) and *cdk1-as1 bnr1Δ* Abp140-3×GFP Abp1-mRFP cells (*Lower*). Abp1-mRFP allowed cells carrying the *cdk1-as1* allele to be distinguished from *CDK1* cells, because the two cell types were co-cultured to insure identical growth and imaging conditions. Cells first were arrested by incubation in HU for 3 h and then were treated with DMSO for 30 min before imaging. Asterisks indicate the start and end points for actin cable elongation.

Movie S2

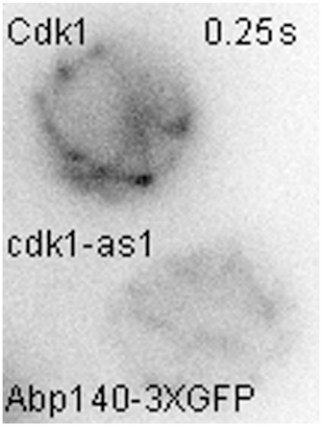

Movie S3. Cdk1 inhibition affects actin cable-assembly rate and signal intensity. The actin cable-assembly rate was assessed by imaging Abp140-3×GFP at the cortex of mother cells of *CDK1 bnr1Δ* Abp140-3×GFP Bni1-3XmCherry (*Upper*) and *cdk1-as1 bnr1Δ* Abp140-3×GFP Abp1-mRFP cells (*Lower*). Cells first were arrested by incubation in HU for 3 h and subsequently were treated with 20 μM 1-NM-PP1 for 30 min before imaging. Asterisks indicate the start and end points for actin cable elongation.

Movie S3

Dataset S1. MS data for actin cable-reconstitution sample

Dataset S1

Polystyrene beads coated with GST-Bni1 FH1-COOH were added to a cell extract prepared from hydroxyurea-synchronized cells.

Dataset S2. Analysis of the MS data for an actin cable-reconstitution sample using the PeptideAtlas database as a reference

Dataset S2

Dataset S3. Description of the significantly enriched protein components from the actin cable-reconstitution sample using the GO annotation

Dataset S3

The description was generated using Osprey software.